J. Fluid Mech. (2009), *vol.* 626, *pp.* 111–147.
doi:10.1017/S0022112008005648 Printed in the United Kingdom

On shear sheltering and the structure of vortical modes in single- and two-fluid boundary layers

TAMER A. ZAKI† AND SANDEEP SAHA
Mechanical Engineering, Imperial College, London SW7 2AZ, UK

(Received 11 June 2008 and in revised form 17 December 2008)

Studies of vortical interactions in boundary layers have often invoked the continuous spectrum of the Orr–Sommerfeld (O-S) equation. These vortical eigenmodes provide a link between free-stream disturbances and the boundary-layer shear – a link which is absent in the inviscid limit due to shear sheltering. In the presence of viscosity, however, a shift in the dominant balance in the operator determines the structure of these eigenfunctions inside the mean shear. In order to explain the mechanics of shear sheltering and the structure of the continuous modes, both numerical and asymptotic solutions of the linear perturbation equation are presented in single- and two-fluid boundary layers. The asymptotic analysis identifies three limits: a convective shear-sheltering regime, a convective–diffusive regime and a diffusive regime. In the shear-dominated limit, the vorticity eigenfunction possesses a three-layer structure, the topmost being a region of exponential decay. The role of viscosity is most pronounced in the diffusive regime, where the boundary layer becomes 'transparent' to the oscillatory eigenfunctions. Finally, the convective–diffusive regime demonstrates the interplay between the the accumulative effect of the shear and the role of viscosity. The analyses are complemented by a physical interpretation of shear-sheltering mechanism. The influence of a wallfilm, in particular viscosity and density stratification, and surface tension are also evaluated. It is shown that a modified wavenumber emerges across the interface and influences the penetration of vortical disturbances into the two-fluid shear flow.

1. Introduction

The ability of free-stream vortical disturbances to penetrate boundary layers is curtailed by the mean shear – an inviscid phenomenon known as *shear sheltering*. At finite Reynolds numbers, however, the sheltering mechanism is less effective, and vortical disturbances permeate the shear. The implications are significant in many engineering and environmental flows. For instance, laminar boundary layers become prone to bypass transition even at moderate levels of free-stream turbulence (Morkovin 1969). In atmospheric flows, vortical disturbances due to thermal convection in clouds can penetrate the lower boundary layer and induce high-speed gusts (Nakamura, Kershaw & Grait 1996). In two-fluid shear flows, free-stream disturbances which reach the two-fluid interface appreciably affect the amplification of interfacial modes (Belcher & Hunt 1998). Our objective is therefore to explain vortical-mode penetration into single- and two-fluid boundary layers and

† Email address for correspondence: t.zaki@imperial.ac.uk

to provide a physical understanding of the mechanics of shear sheltering. The starting point of our study is the continuous-spectrum eigenmodes of the Orr–Sommerfeld (O-S) equation and their dependence on the wavenumber, mean shear and viscosity and density stratification.

1.1. *The continuous spectrum*

The presence of a continuous spectrum was conjectured by Jordinson (1971). He computed the eigenspectrum of the O-S equation for a Blasius boundary layer and commented that the decaying modes form a 'gently curving line'. Mack (1976) computed the temporal eigenvalues over a range of Reynolds numbers and wavenumbers and affirmed the existence of the continuous spectrum by reporting the phase speed and growth rate associated with these modes. These initial investigations were numerical. Formal mathematical characterization of the continuous spectrum, and the analytical expression of its dispersion relation, were later presented by Grosch & Salwen (1978).

Unlike the discrete eigenfunctions which decay away from the mean shear, the continuous eigenfunctions remain oscillatory in the free stream and resemble Fourier modes. Inside the shear, they decay with increasing depth. These modes, therefore, establish a link between free-stream vortical disturbances and the boundary layer – a matter of disconcertion in earlier literature in which only a remarkably weak link could be established (Berger & Aroesty 1977).

Since the work of Grosch & Salwen (1978) the continuous-spectrum modes have been widely applied in studies of boundary-layer stability. The idea that decaying eigenmodes of the O-S equation would play such a significant role in our understanding of flow instability, for instance bypass transition, would have left many researchers incredulous in the era of Tollmien (1929) and Schlichting (1933), where the focus of linear stability research was exponentially unstable solutions.

Together with the discrete waves the continuous modes form a complete basis (Salwen & Grosch 1981). Therefore an arbitrary disturbance can be expressed as a superposition of O-S eigenfunctions. The completeness of O-S spectrum has been applied in studies of the evolution of linear disturbances in boundary layers (Salwen & Grosch 1981), perturbation synthesis (Jacobs & Durbin 2001) and disturbance analysis (Tumin 2003).

The influence of a particular component of the continuous spectrum on boundary-layer stability is largely affected by the structure of the eigenfunction and its extent of penetration into the shear. This penetration is wavenumber-dependent and is limited by shear sheltering.

1.2. *Shear sheltering*

The ability of shear to filter high-frequency vortical perturbations is relevant to both laminar and turbulent flows. In the former, the shear shelters the laminar flow from external vortical forcing. A similar filtering influences the interaction of small- and large-scale eddies in turbulent motion (Hunt & Durbin 1999). A scale disparity is, however, required for shear sheltering to be effective. These conditions were satisfied in the work of Grosch & Salwen (1978), where the computed eigenfunctions were high-frequency and, hence, filtered by the mean shear. Their eigenfunctions decayed exponentially at the edge of the boundary layer. Craik (1991) arrived at a similar conclusion by carrying out inviscid analysis of mode shapes, using a piecewise linear mean flow. Despite the difference in Reynolds numbers, both Grosch & Salwen (1978)

and Craik (1991) considered the same asymptotic limit in which the shear dominates the remaining terms in the O-S equation.

Jacobs & Durbin (1998) studied shear sheltering of the continuous O-S modes for a piecewise linear and infinitely deep boundary layer. Their analysis demonstrated that penetration is inversely proportional to the Reynolds number Re and the disturbance frequency ω. Further investigations of mode shapes were primarily numerical and include Maslowe & Spiteri (2001) and Zaki & Durbin (2006) who examined the effect of pressure gradient on the continuous modes. The importance of shear sheltering is also documented experimentally. Hernon, Walsh & McEligot (2007) have demonstrated that the penetration of free-stream vortical disturbances into a transitional boundary layer indeed agrees with the theoretical prediction of Jacobs & Durbin (1998).

Recent studies of stability of two-fluid shear flows, for instance mixing layers (Yecko & Zaleski 2005), highlight the dependence of transient amplification on modal penetration and, in turn, on the frequency dependence of shear sheltering. However, the shape of the continuous-spectrum modes in two-fluid flows and the influence of viscosity and density stratification on shear sheltering have never been addressed in the literature. Instead, the majority of previous research has focused on the discrete Tollmien–Schlichting and interfacial instability waves (Yih 1967; Hooper & Boyd 1983; Hooper & Boyd 1987). In that context, the work of Charru & Hinch (2000) perhaps bears most relevance to the current investigation. They aimed to classify the various *interfacial* waves based on their extent of penetration into the surrounding fluids. A 'phase diagram' of penetration regimes was developed based on the model problem of Couette flow over a wavy wall. Their analysis, however, only considered two-dimensional, neutral waves due to an infinitesimal displacement of the solid–fluid or fluid–fluid boundary. Since their base flow is bounded, only discrete modes were relevant. The behaviour of free-stream vortical modes, or the continuous-spectrum eigenfunctions, and their ability to penetrate two-fluid shear flows was not discussed. This issue will be addressed herein, and a quantitative measure of penetration and its dependence on modal and flow parameters will be presented. Our analysis takes into account the decay rate of the free-stream vortical disturbance. This is shown to have a significant effect on both modal penetration and the structure of the eigenfunction across the interface.

Due to the importance of the continuous spectrum in studies of single- and two-fluid boundary layers, it is essential to understand the physical mechanisms that determine the structure of these eigenmodes. Shear sheltering is one contributing element. While the literature includes interesting observations related to shear sheltering, questions regarding its physical interpretation and effectiveness remain unanswered. For instance, previous studies suggest that shear sheltering is most pronounced in relation to small-scale, or high-frequency, disturbances particularly at high Reynolds number. This view is however inconsistent with the observation that perturbations with high wall-normal wavenumbers can effectively penetrate boundary layers (Zaki & Durbin 2005). Therefore, in this paper, a clear physical explanation of the mechanics of shear sheltering is sought. We also provide a detailed description of the structure of the continuous modes of the O-S equation, which are classified in terms of their ability to penetrate and perturb the boundary layer. Our approach relies on asymptotic analysis of the governing equation for a piecewise linear profile, in both single- and two-fluid boundary layers. These asymptotic solutions are then compared to the numerical solution of the O-S equation for smoothly varying mean flow profiles to demonstrate the validity of the piecewise linear approximation.

This paper is divided into seven sections. The formulation of the single-fluid problem and the closed-form eigensolution for the piecewise linear mean flow are presented in § 2. The relevant asymptotic regimes are examined in § 3 and are followed by a discussion of the physical mechanism of shear sheltering. The formulation of the two-fluid problem is given in § 4. The associated asymptotic regimes in case of viscosity stratification are derived in § 5. The role of density stratification and surface tension are evaluated numerically in § 6, followed by concluding remarks in the last section.

2. The single-fluid theoretical formulation

The study of penetration of vortical modes into shear regions has as a starting point the linear perturbation equations. The O-S equation for the normal-velocity perturbation v is given according to

$$\left[\left(\frac{\partial}{\partial t}+U\frac{\partial}{\partial x}\right)\nabla^2-\frac{\mathrm{d}^2U}{\mathrm{d}y^2}\frac{\partial}{\partial x}-\nu\nabla^4\right]v=0, \tag{2.1}$$

where $U(y)$ is the mean velocity profile. The perturbation-velocity vector is denoted $\boldsymbol{u}=\{u, v, w\}$, and ν is the fluid viscosity. Lengths are non-dimensionalized by the boundary-layer thickness and velocities by the free-stream speed U_∞, so that ν is effectively $1/Re$.

Since the problem of interest is homogeneous in the streamwise and spanwise directions and in time, the normal-mode assumption can be invoked for the perturbation velocities and pressure, for example

$$v(x, y, z, t)=\phi(y)\mathrm{e}^{\mathrm{i}(k_x x+k_z z-\omega t)},$$

where k_x and k_z are the streamwise and spanwise wavenumber; ω is the frequency; and $\phi(y)$ is the normal-velocity eigenfunction. This reduces the O-S equation (2.1) to the following form:

$$\left[(Uk_x-\omega)\left(\frac{\mathrm{d}^2}{\mathrm{d}y^2}-k^2\right)-\frac{\mathrm{d}^2U}{\mathrm{d}y^2}k_x+\mathrm{i}\nu\left(\frac{\mathrm{d}^2}{\mathrm{d}y^2}-k^2\right)^2\right]\phi=0, \tag{2.2}$$

where $k^2\equiv k_x^2+k_z^2$.

2.1. *The continuous spectrum*

The eigenvalue problem (2.2) requires four boundary conditions. At solid surfaces, the perturbation and its gradient must vanish:

$$\phi_{wall}=0; \qquad \left(\frac{\mathrm{d}\phi}{\mathrm{d}y}\right)_{wall}=0.$$

In semi-bounded flows, the O-S equation possesses a finite number of discrete modes and a spectrum of continuous eigenvalues. The discrete modes are obtained by requiring that the perturbation decays in the free stream, $\phi_\infty\to 0$. Grosch & Salwen (1978) introduced the continuous spectrum by relaxing this free-stream condition. Instead they only required that the perturbation remain bounded:

$$|\phi|<\infty; \qquad |d_y\phi|<\infty,$$

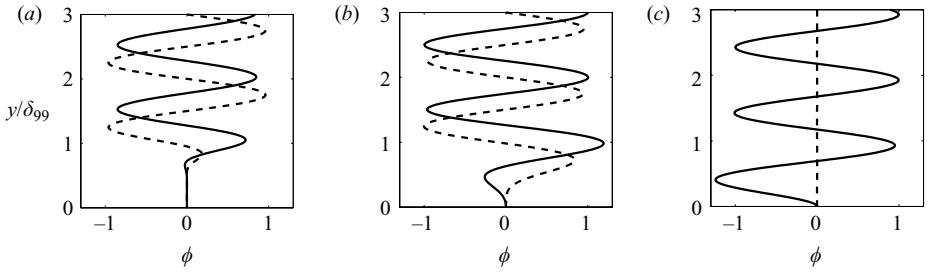

FIGURE 1. Example of continuous-mode shapes for Blasius boundary layer in three different regimes. (*a*) The sheltered regime $k_x Re = 800\pi$, $k_y = 2\pi$, $k_z = 4\pi$; (*b*) the intermediate regime $k_x Re = 50\pi$, $k_y = 2\pi$, $k_z = \pi$; (*c*) the diffusive regime $k_x Re = \pi/100$, $k_y = 2\pi$, $k_z = \pi$; ——, real component; – – –, imaginary component.

where $d_y \equiv \mathrm{d}/\mathrm{d}_y$. The continuous spectrum is obtained from the free-stream behaviour of the O-S equation. In that limit, $d_y U = d_y^2 U = 0$, and the O-S equation reduces to

$$\left[(U_\infty k_x - \omega)\left(\frac{\mathrm{d}^2}{\mathrm{d}y^2} - k_x^2 - k_z^2\right) + \mathrm{i}\nu\left(\frac{\mathrm{d}^2}{\mathrm{d}y^2} - k_x^2 - k_z^2\right)^2\right]\phi_\infty = 0, \tag{2.3}$$

The constant coefficient equation admits solutions of the form $\phi_\infty \sim \mathrm{e}^{\lambda y}$. Substituting $\mathrm{e}^{\lambda y}$ in (2.3) and solving for λ yields the following roots:

$$\lambda_{1,2}^2 = k_x^2 + k_z^2 + \mathrm{i}\frac{k_x}{\nu}(U_\infty - \omega/k_x),$$
$$\lambda_{3,4}^2 = k_x^2 + k_z^2.$$

The oscillatory free-stream solution is obtained by setting $\lambda_{1,2}^2 = -k_y^2$ and, hence, $\phi_\infty \sim \mathrm{e}^{\pm \mathrm{i}k_y y}$. The dispersion relation is therefore

$$-k_y^2 = k_x^2 + k_z^2 + \mathrm{i}\frac{k_x}{\nu}(U_\infty - \omega/k_x),$$

which can be solved for the eigenvalues. In the temporal problem,

$$\omega = k_x U_\infty - \mathrm{i}\nu\left(k_x^2 + k_z^2 + k_y^2\right). \tag{2.4}$$

Assuming the dispersion relation (2.4), the continuous modes are obtained by numerical solution of (2.2). The solution algorithm is an extension of the spectral collocation method of Orszag (1971): Chebyshev polynomials were used to expand the eigenfunctions in the wall-normal direction. Since the polynomials are valid in the domain $[-1, 1]$, nonlinear mapping was incorporated to extend the method to semi-infinite domains. The boundedness condition in the free stream was enforced using the method proposed by Jacobs & Durbin (1998).

The numerical and analytical results presented herein are for three-dimensional disturbances. This choice is motivated by the importance of oblique waves in the transient growth phenomenon in shear flows. Since waves with spanwise wavelengths of the order of the shear thickness are often the most amplified (e.g. Butler & Farrell 1992), the value of $k_z \sim \pi$ is selected for the numerical evaluations of solutions and discussion.

The shapes of three continuous modes for a Blasius base flow are shown in figure 1. The mode shapes suggest that penetration of the vortical mode into the boundary layer is dependent on parameters of the mean flow and of the eigenmode considered.

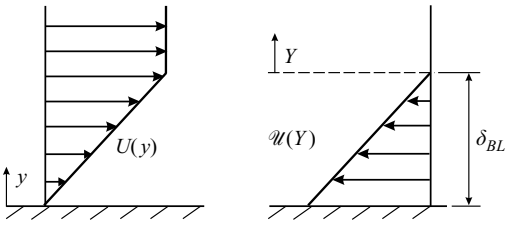

FIGURE 2. Schematic of the single-fluid piecewise linear mean velocity profile. At right, the mean velocity profile is shown in a frame translating at U_∞.

The three modes epitomize three regimes: a sheltered regime in which the free-stream vorticity does not penetrate the boundary layer (figure 1*a*); an intermediate regime in which the vortical perturbation penetrates the boundary layer but not sufficiently to influence the near-wall region (figure 1*b*); and a diffusive regime in which the oscillatory free-stream behaviour of the perturbation persists deep inside the boundary layer in the vicinity of the wall (figure 1*c*). In order to investigate those asymptotic regimes, a piecewise linear base flow is considered in the analyses.

2.2. *Analytical solution for piecewise linear profile*

The numerical solution of the fourth-order O-S equation demonstrates the dependence of the shape of continuous modes on frequency, wavenumber and Reynolds number. However, the mechanisms that determine the structure of the eigenfunction are not evident. Therefore, in order to derive the relevant asymptotic regimes, a piecewise linear mean flow profile is assumed, and the O-S equation is thus reduced to a second-order vorticity equation. This simplification enables us to identify the parameters which determine the structure of the continuous modes. A similar approach was adopted by Craik (1991) in order to explain the results of Grosch & Salwen (1978) for a Blasius profile. First, we present closed-form solutions of the vorticity equation, followed by a discussion of the dominant balances of the equation.

A transformed wall-normal coordinate $Y = y - \delta_{BL}$ is adopted, and the analysis is carried out in a frame translating with the free-stream velocity, $\mathscr{U}(Y) = U(Y) - U_\infty$ as shown in figure 2. The mean flow is therefore

$$\begin{aligned} &\mathscr{U}(Y) = 0, \quad && Y > 0, \\ &\mathscr{U}(Y) = \tau Y, \quad && 0 \geqslant Y \geqslant -\delta_{BL}, \end{aligned} \tag{2.5}$$

where δ_{BL} is the single-fluid boundary-layer thickness and $\tau = U_\infty/\delta_{BL}$.

Using the piecewise linear profile and the dispersion relation (2.4), the final linear stability equations have the form

$$d_Y^2\psi + k_y^2\psi = 0, \quad Y > 0, \tag{2.6}$$

$$d_Y^2\psi + k_y^2\psi - \frac{\mathrm{i}k_x\tau}{\nu}Y\psi = 0, \quad 0 \geqslant Y \geqslant -\delta_{BL}, \tag{2.7}$$

where $\psi \equiv (d_Y^2 - k^2)\phi$. For two-dimensional disturbances, $\psi = (\partial/\partial x)(\partial v/\partial x - \partial u/\partial y)$ is a measure of the spanwise vorticity of a two-dimensional eigenmode. It should be noted that the O-S equation (2.7) in terms of ψ is identical to the homogeneous Squire equation for normal vorticity. Therefore, the shape of the continuous O-S and Squire modes are similar. In addition, asymptotic analyses performed in subsequent sections using (2.7) are also valid for the Squire equation.

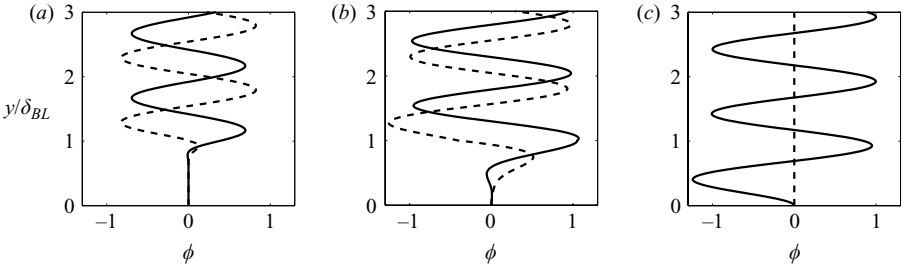

FIGURE 3. Example of continuous-mode shapes for piecewise linear profile in three different regimes: (*a*) convective shear-sheltering regime $k_x Re = 800\pi,\ k_y = 2\pi,\ k_z = 4\pi$; (*b*) convective–diffusive regime $k_x Re = 50\pi,\ k_y = 2\pi,\ k_z = \pi$; (*c*) diffusive regime $k_x Re = \pi/100, k_y = 2\pi,\ k_z = \pi$; ———, real component; – – –, imaginary component.

For the piecewise linear profile, apart from the free-stream and wall boundary conditions, four interface conditions are required in order to match the solutions across the edge of the boundary layer. These conditions are derived from continuity of velocity and stresses,

$$\left.\begin{aligned} \phi(0^+) - \phi(0^-) = 0; \quad & d_Y\phi(0^+) - d_Y\phi(0^-) = \frac{k_x\tau\phi(0)}{k_xU(0)-\omega} \\ d_Y^2\phi(0^+) - d_Y^2\phi(0^-) = 0; \quad & d_Y^3\phi(0^+) - d_Y^3\phi(0^-) = 3k^2\frac{k_x\tau\phi(0)}{k_xU(0)-\omega}. \end{aligned}\right\} \tag{2.8}$$

In the free stream, (2.6) is solved for ψ_{FS} and in turn ϕ_{FS},

$$\psi_{FS} = C_1^{'}\exp(-\mathrm{i}k_yY) + C_2^{'}\exp(\mathrm{i}k_yY), \tag{2.9}$$

$$\phi_{FS} = C_1\exp(-\mathrm{i}k_yY) + C_2\exp(\mathrm{i}k_yY) + C_3\exp(-kY) + C_4\exp(kY) \tag{2.10}$$

(Note that throughout this paper, the subscripts $m = 1,\ 2,\ 3,\ 4$ will be reserved for the integration constants in the free stream, while $m \geqslant 5$ will be used for the solution inside the boundary layer.) In order to maintain boundedness of the eigenfunction in the free stream, $C_4 = 0$. Inside the boundary layer, the solution to (2.7) yields

$$\psi = C_5\mathrm{Ai}[\mathscr{Z}(Y)] + C_6Bi[\mathscr{Z}(Y)], \tag{2.11}$$

$$\begin{aligned} \phi = {} & \exp(-kY)\int_{-\delta_{BL}}^{Y}\exp(ks)(C_5\mathrm{Ai}[\mathscr{Z}(s)] + C_6\mathrm{Bi}[\mathscr{Z}(s)])\,\mathrm{d}s \\ & + \exp(kY)\int_{Y}^{0}\exp(-ks)(C_5\mathrm{Ai}[\mathscr{Z}(s)] + C_6\mathrm{Bi}[\mathscr{Z}(s)])\,\mathrm{d}s \\ & + C_7\exp(-kY) + C_8\exp(kY), \end{aligned} \tag{2.12}$$

where $\mathscr{Z}(Y) = \exp(\mathrm{i}5\pi/6)(k_x\tau/\nu)^{1/3}(Y\ + \mathrm{i}k_y^2\nu/k_x\tau)$. The constants of integration C_m are given in the § A.1 of Appendix A.

Three continuous O-S eigenfunctions evaluated using the above analytic solution are shown in figure 3. Similar to the Blasius eigenfunctions of figure 1, three degrees of modal penetration are observed. These are not, however, evident in the exact analytical expressions (2.11) and (2.12) in which the solution is in terms of integrals of the Airy functions. In the following section, the O-S equation (2.7) inside the

boundary layer is revisited,

$$d_Y^2\psi + k_y^2\psi - \frac{\mathrm{i}k_x\tau}{\nu}Y\psi = 0, \tag{2.13}$$

and asymptotic solutions are derived based on the relative magnitude of the convective term $\mathrm{i}k_x\tau Y$ and diffusive term νk_y^2. The objective is to explain the different mechanisms governing vortical-mode penetration inside the boundary layer. Three limits are considered and will be referred to as

(*a*) the convective, shear-sheltered regime, $k_x\tau\delta_{BL}/\nu k_y^2 \gg 1$;

(*b*) the diffusive regime, $k_x\tau\delta_{BL}/\nu k_y^2 \ll 1$; and

(*c*) the convective–diffusive regime, $k_x\tau\delta_{BL}/\nu k_y^2 \sim O(1)$.

3. Asymptotic solutions in the single-fluid boundary layer

3.1. *The convective shear-sheltered regime*

Hunt (1977) and co-workers investigated the interaction of vortical disturbances with shear flows. Their inviscid rapid distortion theory (RDT) solution demonstrated that all free-stream vortical disturbances are simply convected and do not penetrate the shear. The result was disconcerting because it did not allow any interaction of the free-stream disturbances with the boundary-layer shear. The inability of the shear region to sustain a vortical solution is due to the inviscid assumption. When $\nu = 0$, the vorticity equation (2.7) reduces to, $\mathrm{i}k_x(c - U(Y))\psi = 0$. A non-trivial solution requires that the phase speed of the vortical disturbance equals that of the base flow. For the continuous-spectrum modes, $c = U_\infty$, and therefore these disturbances can only be sustained in the free stream.

Jacobs & Durbin (1998) incorporated the effect of viscosity in their analysis of the continuous modes. They demonstrated that viscous theory allows for vortical penetration into the shear and that the penetration depth is proportional to $(\nu/\omega\tau)^{1/3}$. Zaki & Durbin (2005) extended this analysis in order to incorporate the modal decay rate.

All the above analyses only considered high-frequency disturbances in an infinitely deep boundary layer. The effect of the wall on modal penetration was not included. Here, a finite-thickness boundary layer is considered in order to demonstrate both shear sheltering and the blocking effect of the wall. A small parameter $\epsilon_s \equiv \nu k_y^2/k_x\tau\delta_{BL} \ll 1$ is defined; the subscript s denotes the shear-sheltered regime. Equation (2.7) can be expressed in terms of the small parameter,

$$\epsilon_s d_Y^2\psi + \epsilon_s k_y^2\psi - k_y^2\frac{\mathrm{i}Y}{\delta_{BL}}\psi = 0.$$

A series expansion $\psi = \epsilon_s^0\psi_0 + \epsilon_s^1\psi_1 + \epsilon_s^2\psi_2 + \cdots$ yields trivial solutions for all powers of ϵ_s. This solution, while possibly valid in the bulk of the shear, cannot match the free-stream vorticity, nor can it satisfy the wall boundary conditions; indeed $\psi = 0$ in the near-wall region violates both the no-penetration and no-slip boundary conditions. Therefore, an *edge* and a *wall* layer develop in these regions of the shear in order to satisfy the free-stream matching and wall boundary conditions, respectively.

In the edge layer, a scaled coordinate $Y_e \equiv Y/\delta_e$, and $\psi_e \equiv \psi(Y)$ are introduced, and the governing equation becomes

$$\frac{\epsilon_s}{\delta_e^2}\frac{\mathrm{d}^2\psi_e}{\mathrm{d}Y_e^2} + \epsilon_s k_y^2\psi_e - \mathrm{i}k_y^2\frac{\delta_e}{\delta_{BL}}Y_e\psi_e = 0. \tag{3.1}$$

Balance of the dominant terms implies that $\delta_e \sim O(\nu/k_x\tau)^{1/3}$. To leading order, this scaling yields

$$\frac{\mathrm{d}^2\psi_e}{\mathrm{d}Y_e^2} - \mathrm{i}Y_e\psi_e = 0,$$

and hence the solution is given by

$$\psi_e = C_{e_1}\mathrm{Ai}[\exp(\mathrm{i}5\pi/6)Y_e] + C_{e_2}\mathrm{Bi}[\exp(\mathrm{i}5\pi/6)Y_e]. \tag{3.2}$$

In the limit $Y_e \to -\infty$, the edge-layer solution ψ_e must asymptotically match the trivial solution in the bulk of the shear, which leads to $C_{e_2} = 0$.

In the wall layer, the scaled coordinate $Y_w \equiv (\delta_{BL} + Y)/\delta_w$ and $\psi_w \equiv \psi(Y)$ are introduced. The governing equation rewritten in terms of wall coordinates is therefore

$$\frac{1}{\delta_w^2}\frac{\mathrm{d}^2\psi_w}{\mathrm{d}Y_w^2} + \frac{\mathrm{i}k_x\tau}{\nu}(\delta_{BL}(1 - \mathrm{i}\epsilon_s) - \delta_w Y_w)\psi_w = 0. \tag{3.3}$$

Expanding ψ_w in powers of ϵ_s and balancing the leading-order terms gives $\delta_w \sim O(\sqrt{\frac{\nu}{k_x\tau\delta_{BL}}})$. To the leading order, the governing equation is

$$\frac{\mathrm{d}^2\psi_w}{\mathrm{d}Y_w^2} + \mathrm{i}\psi_w = 0. \tag{3.4}$$

The leading order solution is therefore

$$\psi_w(Y_w) = C_{w_1}\exp\left(\frac{1}{\sqrt{2}}(1 - \mathrm{i})Y_w\right) + C_{w_2}\exp\left(-\frac{1}{\sqrt{2}}(1 - \mathrm{i})Y_w\right). \tag{3.5}$$

The above expression must asymptotically match the trivial solution in the bulk of the shear, $\lim_{Y_w\to\infty}\psi_w(Y_w) = 0$, and therefore $C_{w_1} = 0$.

A uniformly valid vorticity eigenfunction can be expressed in terms of the bulk, edge and wall-layer solutions. To the leading order, in the shear region $Y \in [-\delta_{BL}, 0]$, the continuous mode is given by

$$\psi = C_{e_1}\mathrm{Ai}[\varsigma(Y)] + C_{w_2}\exp(-\zeta(\delta_{BL} + Y)), \tag{3.6}$$

where $\varsigma(Y) = \exp(\mathrm{i}5\pi/6)(k_x\tau/\nu)^{1/3}Y$ and $\zeta = (1 - \mathrm{i})/\sqrt{2}\delta_w$. The normal-velocity eigenfunction inside the boundary layer is therefore

$$\begin{aligned}\phi = {} & C_5\exp(-kY) + C_6\exp(kY) + C_{w_2}\exp(-\zeta(\delta_{BL} + Y)) \\ & + C_{e_1}\left[\exp(-kY)\int_{-\delta_{BL}}^{Y}\exp(ks)\mathrm{Ai}[\varsigma(s)]\,\mathrm{d}s\right. \\ & \left. + \exp(kY)\int_{Y}^{0}\exp(-ks)\mathrm{Ai}[\varsigma(s)]\,\mathrm{d}s\right].\end{aligned} \tag{3.7}$$

The constants of integration can be evaluated using the boundary and matching conditions and are given in § A.2 of Appendix A. The eigenfunction (3.7) is composed of an exponentially decaying component and an integral of the airy function which is decaying for $Y < 0$. The coefficient of the exponentially growing component is very small according to (A 2), and therefore its contribution is negligible.

A comparison of the mode shapes from the shear-sheltered asymptotic limit and the exact eigenfunction (2.12) is not included because the two solutions coincide nearly identically in this regime. Instead, figures 4 and 5 compare the eigenfunctions

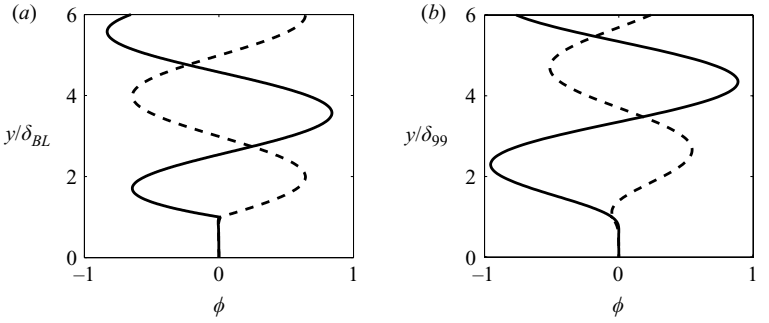

FIGURE 4. Continuous-mode shape in convective shear-sheltered regime for (*a*) piecewise linear profile and (*b*) Blasius boundary layer: ———, real component; – – –, imaginary component; $k_x Re = 1000,\ k_y = \pi,\ k_z = \pi/3$.

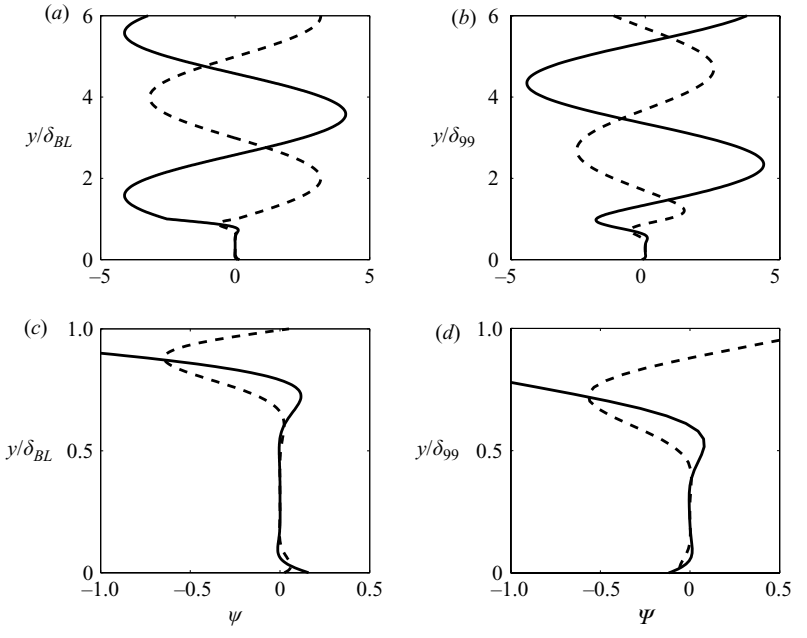

FIGURE 5. Spanwise vorticity in the convective shear-sheltered regime. (*a*), (*c*) Eigenfunction for piecewise linear profile; (*b*), (*d*) eigenfunction for Blasius boundary layer; (*c*), (*d*) The eigenfunction ψ inside the boundary layer; ———, real component; – – –, imaginary component; $k_x Re = 1000,\ k_y = \pi,\ k_z = \pi/3$.

ϕ and ψ for a piecewise linear profile to those obtained for a Blasius mean flow. The eigenfunction ϕ is oscillatory in the free stream and decays rapidly inside the boundary layer, indicating the strong influence of shear, $\epsilon_s \equiv \nu k_y^2 / k_x \tau \delta_{BL} \ll 1$. The decay in the eigenfunction of the piecewise linear profile is more rapid near the edge of the boundary layer due to the higher level of shear in comparison to the Blasius mean flow.

More insight into the structure of these vortical modes can be gathered from figure 5. In the free stream the vorticity ψ is oscillatory. Inside the boundary layer, shown in the bottom pane of figure 5, three regions can be clearly identified:

(*a*) the outer layer near the edge of the boundary layer;

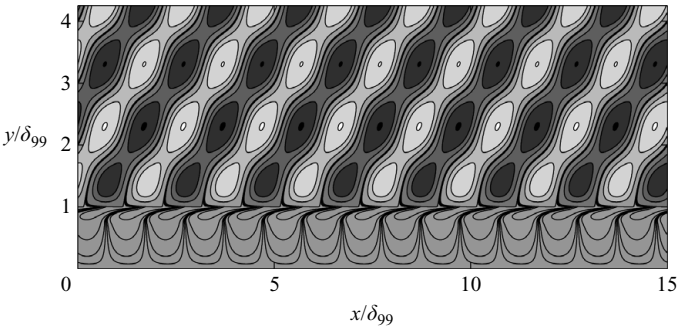

FIGURE 6. Streamlines of a continuous mode with $k_x Re = 1000\pi$, $k_y = \pi$, $k_z = 0$.

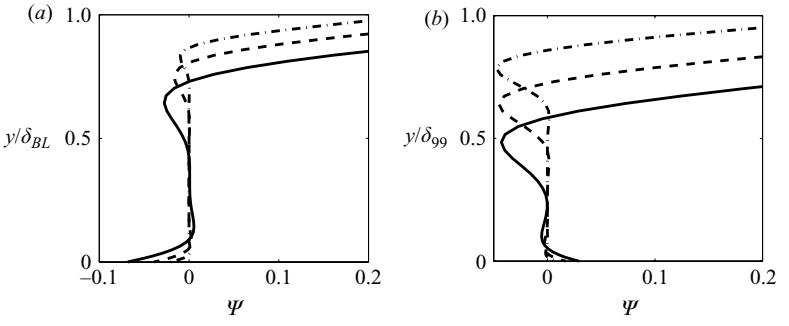

FIGURE 7. Effect of Reynolds number on spanwise vorticity for (*a*) piecewise linear profile and (*b*) Blasius boundary layer; $k_x = \pi$, $k_y = \pi$, $k_z = \pi$; ———, $Re = 100$; – – –, $Re = 200$; — · —, $Re = 1000$.

(*b*) the bulk, or central region, which is devoid of any significant vortical disturbance; and

(*c*) the wall layer in which vorticity is again non-zero.

The scaling of these layers is captured by the above-derived asymptotic solutions. The outer layer is a measure of the extent of penetration of the free-stream vorticity into the shear. Its thickness is $\delta_e \propto (\nu/k_x\tau)^{1/3}$. Beyond δ_e, the shear prevents further penetration of the free-stream mode. The vortical disturbance in the outer layer is convected downstream and imposes a normal-velocity 'boundary condition' on the bulk of the shear. As a result, an exponentially small, irrotational perturbation field is set up in that region. While this inviscid mechanism is relevant to the other asymptotic regimes discussed in this work, it is most discernible in the shear-sheltered eigenfunctions. In this limit, viscous penetration of the free-stream disturbance is inhibited, and as a result, the contribution of the inviscid mechanism to the eigenfunction inside the shear is more evident. An example of the streamlines is shown in figure 6. In the vicinity of the wall, vorticity is generated in order to satisfy the no-slip and no-penetration boundary conditions. The wall layer is in fact a Stokes layer whose length scale is $\delta_w \sim \sqrt{\nu/\Omega}$, where $\Omega \equiv k_x U_\infty$ is the frequency of oscillation of the free stream.

The effect of viscosity on the edge- and wall-layer thicknesses is shown in figure 7. This behaviour is captured by the expressions for the length scales δ_w and δ_e. It is instructive to consider two sources of vorticity: the first in the free stream and the second at the wall. At low viscosity, scaling δ_{BL} by the edge layer $\delta_e \propto (\nu/k_x\tau)^{1/3}$,

the boundary layer appears deeper, and hence, there is no overlap between the free stream and wall-generated vorticity. Lowering the viscosity causes the sources to move further apart, thus widening the inner core. In the limit $\nu \to 0$, the influence of the wall becomes insignificant.

It is important to note that the decay of the eigenfunction inside the boundary layer is due to the sheltering effect of the shear and is not a wall-blocking phenomenon. This can be further verified by considering the limit of infinite shear, $\delta_{BL} \to \infty$. In this limit, the eigenfunction (3.7) reduces to

$$\phi = C_5 \exp(kY) + C_{e_1}\left[\exp(-kY)\int_{-\infty}^{Y} \exp(ks)\mathrm{Ai}[\varsigma(s)]\,\mathrm{d}s + \exp(kY)\int_{Y}^{0} \exp(-ks)\mathrm{Ai}[\varsigma(s)]\,\mathrm{d}s\right] \quad (3.8)$$

or equivalently $\psi = C_{e_1}\mathrm{Ai}[\varsigma(Y)]$. A similar expression for ψ was obtained by Jacobs & Durbin (1998) for the infinitely deep boundary layer. The normal-velocity eigenfunction (3.8) is composed of an exponentially decaying component and the integral of first airy function which is also decaying. Therefore, in the absence of a solid boundary, the normal velocity is exponentially small but not exactly zero. A solid boundary at finite Y forces ϕ to be zero, and therefore, spanwise vorticity, ψ, must be generated at the wall in order to satisfy the boundary conditions. The extent of diffusion of this wall vorticity into the shear is the thickness of the wall layer δ_w.

3.2. *The diffusive regime*

The reciprocal of the shear-sheltered limit is the diffusive regime. In this regime, the filtering effect of the shear is ineffective, and the oscillatory free-stream vortical disturbances persist deep into the boundary layer (figure 3*c*). As the name suggests, the viscosity dominates the convective term in the continuous-mode vorticity equation (2.7). A small parameter $\epsilon_d \equiv k_x \tau \delta_{BL}/\nu k_y^2 \ll 1$ can be defined. The vorticity equation (2.7) can therefore be expressed in terms of ϵ_d,

$$\frac{1}{k_y^2} d_Y^2 \psi + \psi - \epsilon_d \frac{\mathrm{i}Y}{\delta_{BL}}\psi = 0.$$

Assuming a power series solution, $\psi \sim \psi_0 + \epsilon_d \psi_1 + \epsilon_d^2 \psi_2 + \cdots$, the governing equation to leading order has the form

$$\frac{1}{k_y^2} d_Y^2 \psi + \psi = 0. \quad (3.9)$$

The above equation resembles the governing equation for Stokes second problem. However, unlike the real frequency of oscillation in the Stokes problem, the oscillatory behaviour of the continuous modes is in the wall-normal direction due to k_y dependence in the free stream.

The solution to the leading-order vorticity equation and the corresponding wall-normal-velocity perturbation ϕ are, respectively,

$$\left.\begin{aligned} \psi &= C_5' \exp(-\mathrm{i}k_y Y) + C_6' \exp(\mathrm{i}k_y Y), \\ \phi &= C_5 \exp(-\mathrm{i}k_y Y) + C_6 \exp(\mathrm{i}k_y Y) + C_7 \exp(-kY) + C_8 \exp(kY). \end{aligned}\right\} \quad (3.10)$$

The constant C_5 through C_8 are obtained by satisfying the wall boundary conditions and matching conditions at the edge of the boundary layer, and are provided in § A.3 of Appendix A. For $k_x = 0$, the similarity between the above expression for ϕ and the

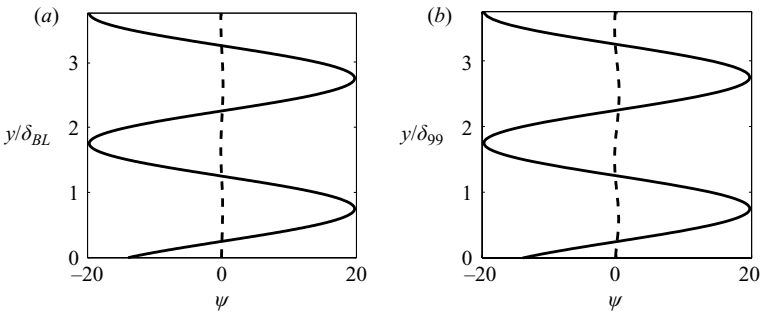

FIGURE 8. Continuous-mode shapes in the diffusive regime. (*a*) Eigenfunctions for piecewise linear profile and (*b*) eigenfunctions for Blasius boundary layer; ———, real component; – – –, imaginary component; $k_x Re = \pi/10,\ k_y = \pi,\ k_z = \pi$.

free-stream eigenfunction (2.10) can be exploited in order to derive a uniformly valid solution for $Y \in [-\delta_{BL}, \infty)$,

$$\phi = C\exp(-k\delta_{BL})\left[\exp(-kY) - \frac{1}{2}\left(1 + \frac{k}{\mathrm{i}k_y}\right)\exp(k\delta_{BL} - \mathrm{i}k_y(\delta_{BL} + Y)) - \frac{1}{2}\left(1 - \frac{k}{\mathrm{i}k_y}\right)\exp(k\delta_{BL} + \mathrm{i}k_y(\delta_{BL} + Y))\right], \quad (3.11)$$

where C is the arbitrary amplitude of the free-stream vortical mode.

The most conspicuous attribute of the modes is their ability to preserve the free-stream oscillatory nature throughout the boundary-layer shear, to the wall. This behaviour is characteristic of streamwise-elongated, or low-k_x, vortical modes, as suggested by the scaling parameter $\epsilon_d \equiv k_x \tau \delta_{BL}/\nu k_y^2$. The expression for ϵ_d also suggests that high k_y belong to the diffusive regime and can therefore penetrate the boundary layer. This observation is consistent with Zaki & Durbin (2005).

Figure 8 compares the mode shapes obtained from the asymptotic solution (3.10) for a piecewise linear profile to that obtained for a Blasius boundary layer. In addition to the similarity in the mode shape, good quantitative agreement is also observed. This agreement can be explained by noting that the terms associated with the mean flow in the O-S equation (the convective and mean curvature terms) are an order of magnitude smaller than the viscous and transient terms. The leading-order O-S equation therefore is independent of the mean flow chosen, and as a result, we observe good quantitative agreement between the eigenfunctions shown in figure 8.

3.3. *The convective–diffusive regime*

Free-stream vortical modes which partially penetrate the boundary-layer shear (figure 3*b*) do not fall within the premise of the fully sheltered convected disturbances or of the fully penetrating viscous regime. Instead, in the convective–diffusive regime, both the convective and viscous terms in the vorticity equation (2.7) are of comparable magnitude throughout the bulk of the shear, $k_x \tau \delta_{BL} \sim \nu k_y^2$. The structure of the eigenfunctions is examined by considering solutions of the vorticity equation in the outer region of the boundary layer and in the vicinity of the wall.

Near the edge of the boundary layer, $Y \to 0$, the vorticity equation (2.7) is approximated to the lowest order in Y by the diffusion dominated limit,

$$\frac{\mathrm{d}^2\psi_e^0}{\mathrm{d}Y^2} + k_y^2\psi_e^0 = 0,$$

whose solution is given according to

$$\psi_e^0 = \underbrace{C_{e_1}\exp(\mathrm{i}k_y Y)}_{\psi_{e_1}^0} + \underbrace{C_{e_2}\exp(-\mathrm{i}k_y Y)}_{\psi_{e_2}^0}. \tag{3.12}$$

This oscillatory solution mimics the free-stream eigenfunction exactly, and shear sheltering is negligible near the edge of the boundary layer. The influence of the uniform shear is therefore *not* local but, as suggested by the convective term $k_x \tau Y$, cumulative with increased depth within the boundary layer.

In order to demonstrate the influence of the shear on the wall-normal decay of the eigenfunction, a correction is sought for each of the two independent solutions $\psi_{e_1}^0$ and $\psi_{e_2}^0$ (the procedure is outlined for $\psi_{e_1}^0$ only). The corrected solution $\psi_{e_1} = \psi_{e_1}^0 + \psi_{e_1}^1$, where $\psi_{e_1}^1 \ll \psi_{e_1}^0$, is substituted in the vorticity equation (2.7), and the following equation for $\psi_{e_1}^1$ is obtained:

$$\frac{\mathrm{d}^2\psi_{e_1}^1}{\mathrm{d}Y^2} + k_y^2\psi_{e_1}^1 - \frac{\mathrm{i}k_x\tau Y}{\nu}C_{e_1}\mathrm{e}^{+\mathrm{i}k_y Y} = 0,$$

with the homogeneous boundary conditions $\psi_{e_1}^1 = d_Y\psi_{e_1}^1 = 0$ at $Y = 0$. The correction term is therefore

$$\psi_{e_1}^1 = C_{e_1}\mathrm{e}^{\mathrm{i}k_y Y}\left[\frac{k_x\tau}{2k_y\nu}\left(\frac{Y^2}{2} - \frac{Y}{2\mathrm{i}k_y} - \frac{1-\mathrm{e}^{-2\mathrm{i}k_y Y}}{4k_y^2}\right)\right].$$

A similar procedure yields the correction $\psi_{e_2}^1$, and finally the asymptotic behaviour of the vorticity eigenfunction near $Y = 0$ can be expressed as

$$\begin{aligned}\psi_e(Y) = \underbrace{C_{e1}\mathrm{e}^{\mathrm{i}k_y Y}}_{\psi_{e_1}^0} + \underbrace{C_{e_1}\mathrm{e}^{\mathrm{i}k_y Y}\left[\frac{k_x\tau}{2k_y\nu}\left(\frac{Y^2}{2} - \frac{Y}{2\mathrm{i}k_y} - \frac{1-\mathrm{e}^{-2\mathrm{i}k_y Y}}{4k_y^2}\right)\right]}_{\psi_{e_1}^1} \\ + \underbrace{C_{e2}\mathrm{e}^{-\mathrm{i}k_y Y}}_{\psi_{e_2}^0} + \underbrace{C_{e_2}\mathrm{e}^{-\mathrm{i}k_y Y}\left[-\frac{k_x\tau}{2k_y\nu}\left(\frac{Y^2}{2} + \frac{Y}{2\mathrm{i}k_y} - \frac{1-\mathrm{e}^{2\mathrm{i}k_y Y}}{4k_y^2}\right)\right]}_{\psi_{e_2}^1}.\end{aligned} \tag{3.13}$$

The constants C_{e1} and C_{e2} are obtained by matching the vorticity and its gradient at the edge of the boundary layer. These constants have been provided in § A.4 of Appendix A.

In the approximate solution (3.13), both $\psi_{e_1}^0$ and $\psi_{e_2}^0$ are oscillatory and only account for the diffusive term. The decay of the eigenfunction inside the boundary layer is due to an incomplete cancellation by the increasing amplitudes of $\psi_{e_1}^1$ and $\psi_{e_2}^1$ inside the shear, $Y < 0$. The decay of the solution inside the boundary layer is captured in figure 9. The figure compares the exact and asymptotically derived vorticity eigenfunctions. The two solutions are in good quantitative agreement in the region $0.6 < y/\delta_{BL} < 1$. The oscillation of the eigenfunction near the edge of the boundary layer and the gradual decay in the amplitude of oscillation due to the cumulative effect of the shear are captured by (3.13).

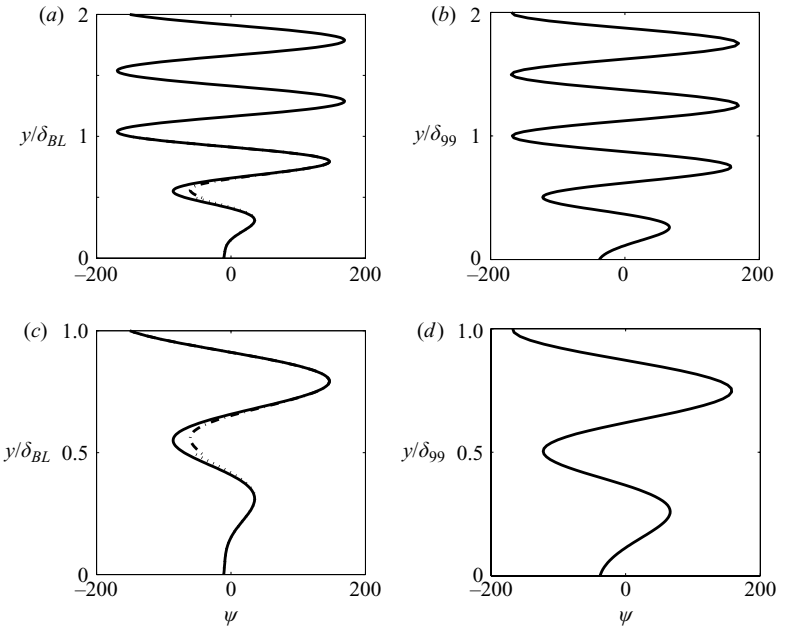

FIGURE 9. Spanwise vorticity in the convective–diffusive regime. (*a*), (*c*) Re(ψ) for a piecewise linear profile and (*b*), (*d*) Re(ψ) for a Blasius boundary layer; ———, exact analytical solution; —·—, oscillatory solution; ·····, exponential wall solution; $k_x Re = 50\pi$, $k_y = 4\pi$, $k_z = \pi$.

The near-wall behaviour of the eigenfunction is derived by considering the limit $Y \to -\delta_{BL}$ of the vorticity equation (2.7),

$$\frac{\mathrm{d}^2\psi_w^0}{\mathrm{d}Y^2} + \left(k_y^2 + \mathrm{i}\frac{k_x\tau\delta_{BL}}{\nu}\right)\psi_w^0 = 0.$$

The lowest order approximation of the vorticity eigenfunction is therefore composed of a growing and a decaying exponential,

$$\psi_w^0 = \underbrace{C_{w_1}\exp(\mathrm{i}\kappa_w(Y+\delta_{BL}))}_{\psi_{w_1}^0} + \underbrace{C_{w_2}\exp(-\mathrm{i}\kappa_w(Y+\delta_{BL}))}_{\psi_{w_2}^0}, \tag{3.14}$$

where $\kappa_w = \sqrt{k_y^2 + \mathrm{i}(k_x\tau\delta_{BL}/\nu)}$. The cumulative effect of the shear over the boundary layer $\mathrm{i}k_x\tau\delta_{BL}/\nu$ determines the deviation of the solution from a purely oscillatory form. In a manner similar to the solution in edge layer, a corrected eigenfunction $\psi_w = \psi_w^0 + \psi_w^1$ is obtained in the wall region:

$$\begin{aligned}\psi_w(Y) = {} & C_{w1}\mathrm{e}^{\mathrm{i}k_w(Y+\delta_{BL})} + C_{w2}\mathrm{e}^{-\mathrm{i}k_w(Y+\delta_{BL})} \\ & + C_{w1}\mathrm{e}^{\mathrm{i}k_w(Y+\delta_{BL})}\left[\frac{k_x\tau}{2k_w\nu}\left(\frac{(Y+\delta_{BL})^2}{2} - \frac{(Y+\delta_{BL})}{2\mathrm{i}k_w} - \frac{1-\mathrm{e}^{-2\mathrm{i}k_w(Y+\delta_{BL})}}{4k_w^2}\right)\right] \\ & + C_{w2}\mathrm{e}^{-\mathrm{i}k_w(Y+\delta_{BL})}\left[\frac{-k_x\tau}{2k_w\nu}\left(\frac{(Y+\delta_{BL})^2}{2} + \frac{(Y+\delta_{BL})}{2\mathrm{i}k_w} - \frac{1-\mathrm{e}^{2\mathrm{i}k_w(Y+\delta_{BL})}}{4k_w^2}\right)\right].\end{aligned}$$

The constants C_{w_1} and C_{w_2} are given in § A.4 of Appendix A and are obtained by imposing continuity of vorticity and its gradient at the wall. Agreement between the asymptotic wall-layer solution ψ_w and the exact eigenfunction is shown in figure 9.

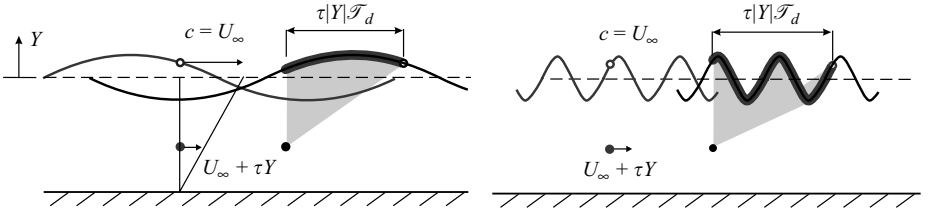

FIGURE 10. Schematic of modal penetration for low- and high-frequency free-stream vortical perturbations.

3.4. *Discussion*

The propensity of a vortical free-stream mode to penetrate the boundary layer is enhanced by the viscosity and limited by the shear. The filtering effect of the shear is, however, wavenumber-dependent. In the limit $\epsilon_s \equiv \nu k_y^2/k_x\tau\delta_{BL} \ll 1$, shear sheltering is most effective. Therefore, high-k_x, or short streamwise-wavelength, vortical modes cannot penetrate the boundary layer. In the reciprocal limit of long streamwise-wavelength, $\epsilon_d \equiv k_x\tau\delta_{BL}/\nu k_y^2 \ll 1$, the eigenfunction preserves its free-stream oscillatory nature and amplitude deep into the boundary layer.

A physical interpretation of shear sheltering is proposed by considering the relative motion of a free-stream vortical mode and a point P within the shear (figure 10). The vortical mode at the edge of the boundary layer convects downstream at $c = U_\infty$, and point P has speed $U(p) = U_\infty + \tau Y$. The influence of the free-stream disturbance reaches P by wall-normal diffusion *only*. Within the diffusion time scale $\mathscr{T}_d \equiv 1/k_y^2\nu$, the free-stream boundary condition which affects P varies due to the relative motion of the wave and the shear flow. As a result, point P is exposed to n wavelengths of the free-stream disturbance, where n is given by

$$n = \frac{(c - U(p))\,\mathscr{T}_d}{1/k_x} = \frac{k_x\tau|Y|}{k_y^2\nu}.$$

The definition of n is a ratio of two time scales: the numerator defines the relative streamwise convection, or shear, time scale according to $\mathscr{T}_s \equiv 1/k_x\tau\delta_{BL}$, and the denominator defines the wall-normal diffusion time scale $\mathscr{T}_d \equiv 1/k_y^2\nu$. For low-$k_x$, or streamwise-elongated, waves, $n \to 0$, and the perturbation at the edge of the boundary layer is seemingly steady relative to point P over the diffusion time scale $\mathscr{T}_d$. As a result, a free-stream vortical mode diffuses effectively into the boundary-layer shear in this limit. On the other hand, for short waves, n tends to ∞, and the edge condition appears to be changing very rapidly with respect to point P. The net effect over the time scale $\mathscr{T}_d$ is a near-zero edge condition relative to point P. As a result, the penetration of high-k_x vortical modes is limited. The filtering effect of high frequencies is enhanced by the shear $n \propto k_x\tau Y$, and hence the terminology 'shear sheltering'. The precise mechanism is due to the difference in convective speeds between the free-stream perturbation and the flow inside the boundary layer. Therefore, shear sheltering is cumulative, and n increases with depth.

When the convection and diffusion terms are approximately equal, $n \sim O(1)$, and the perturbation is able to partially penetrate the boundary layer but decays due to the cumulative influence of the shear. Therefore, the vorticity eigenfunctions in this regime are oscillatory near the edge of the boundary layer and exponentially decaying in the near-wall region.

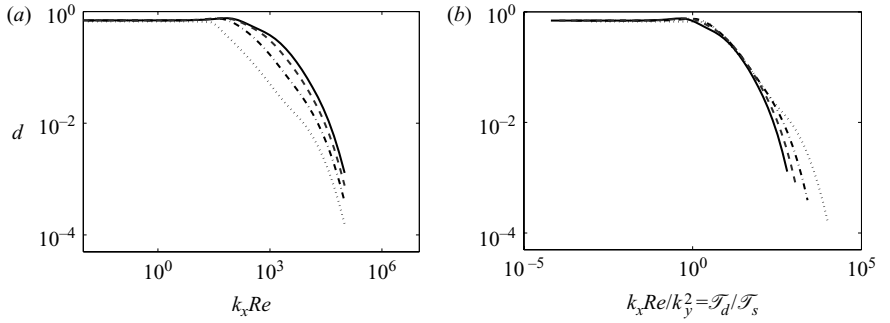

FIGURE 11. Variation in penetration depth with (*a*) $k_x Re$ and (*b*) $k_x Re/k_y^2$; ———, $k_y = 4\pi$; – – –, $k_y = 3\pi$; — · —, $k_y = 2\pi$; ·····, $k_y = \pi$.

The exact analytical expression (2.11) for $\psi(y)$ captures the change in the eigenfunction from oscillatory to exponential decay:

$$\psi = C_5 \mathrm{Ai}\left[\mathscr{Z}(Y)\right] + C_6 \mathrm{Bi}\left[\mathscr{Z}(Y)\right]. \tag{2.11}$$

The ratio of the convective and diffusive time scales $\mathscr{T}_s/\mathscr{T}_d$ appears in the argument of the Airy function,

$$\mathscr{Z}(Y) = \exp\left(\mathrm{i}5\pi/6\right)\left(\frac{Y}{\delta_e} + \mathrm{i}\frac{\mathscr{T}_s \delta_{BL}}{\mathscr{T}_d \delta_e}\right).$$

The ratio $\mathscr{T}_s/\mathscr{T}_d$ determines the phase of $\mathscr{Z}(Y)$ and in turn the behaviour of the Airy solution. In the viscous regime, the diffusive time scale is much shorter than the convective time scale, $\mathscr{T}_d \ll \mathscr{T}_s$. As a result, $|phase(\mathscr{Z})| > \pi/3$, and the first and second Airy functions are both oscillatory. In the shear-sheltered regime, $\mathscr{T}_d \gg \mathscr{T}_s$. Therefore, $\mathrm{i}\mathscr{T}_s\delta_{BL}/\mathscr{T}_d\delta_e \to 0$ and $(|phase(\mathscr{Z})| \sim \pi/6) < \pi/3$. In this region of the complex plane, $\mathrm{Ai}(\mathscr{Z})$ is monotonically decreasing, and $\mathrm{Bi}(\mathscr{Z})$ is increasing. The coefficient of the latter, C_6, is negligible in the sheltered regime, and the overall behaviour of the vorticity eigenfunction is captured by the decaying $\mathrm{Ai}(\mathscr{Z})$.

The shear-sheltered solution is also recovered in the limit of vanishing kinematic viscosity. In this limit, $\mathscr{T}_d \to \infty$ and $\delta_e \to 0$. Since $\mathscr{T}_d \propto 1/\nu$ and $\delta_e \propto \nu^{1/3}$, their product tends to infinity. As a result, the same limit $(|phase(\mathscr{Z})| \sim \pi/6) < \pi/3$ is obtained and the eigenfunction is exponentially decaying.

3.5. *Penetration depth*

In order to quantify the propensity of a continuous mode to permeate the boundary layer, a penetration depth norm is defined:

$$d \equiv \int_0^{\delta_{BL}} \frac{|\phi|}{|\phi|_\infty}\, \mathrm{d}y,$$

where $|\phi|_\infty$ is the free-stream amplitude of the eigenfunction. Figure 11 shows the variation of d with $k_x Re$ for various k_y. In the limit $k_x Re \to \infty$ penetration depth tends to zero. The same behaviour is observed whether $k_x \to \infty$ and Re remains finite or the opposite. In the first case, the boundary layer appears infinitely deep when scaled by the disturbance wavelength, and hence penetration is negligible. When $Re \to \infty$ and k_x is finite, viscous effects can be ignored, and no means of vortical mode penetration in the boundary layer is present. As $k_x Re$ is reduced, penetration increases due to the increase in $\mathscr{T}_s$ compared to $\mathscr{T}_d$. The change in the behaviour of the penetration depth

curve near $k_x Re \sim O(10^2)$ marks the convective–diffusive regime in which both time scales become comparable. At lower $k_x Re$, the diffusive regime is reached and d does not change significantly; the oscillatory solution prevails deep inside the boundary layer. Penetration increases with k_y due to the reduction of the diffusive time scale. In the viscous regime, however, d is maximum and saturates independent of the wall-normal wavenumber.

Motivated by the discussion of the convective and diffusive time scales, the penetration curves are plotted against $n = \mathscr{T}_d/\mathscr{T}_s$ in figure 11(b). Residual dependence of penetration on n is observed in the sheltered regime in which penetration is negligible. However, the penetration curves collapse in the diffusive ($\mathscr{T}_d/\mathscr{T}_s < 1$) and the convective–diffusive ($\mathscr{T}_d/\mathscr{T}_s \sim O(1)$) regimes.

4. The two-fluid theoretical formulation

The shape of the continuous-spectrum modes and their ability to penetrate a single-fluid boundary layer depend on the disturbance wavenumber, the intensity of the mean shear and the kinematic viscosity of the fluid. In two-fluid boundary layers, both the mean shear and viscosity are discontinuous across the two-fluid interface. In addition, the density discontinuity and surface tension appear in the interfacial stress conditions and can, therefore, affect the ability of free-stream disturbances to penetrate the lower film. In order to investigate the dependence of mode shape on these parameter, analyses similar to those carried out in the context of single-fluid boundary layers are presented for the two-fluid problem. First, an exact analytical expression of the eigenfunction is derived assuming a piecewise linear mean flow. The exact solution is subsequently explained by considering possible asymptotic limits.

The O-S equation for immiscible two-fluid flows and the interfacial boundary conditions were given by Yih (1967). Since then the equations have been extended in order to account for the influence of surface tension and density stratification in the interface conditions, as well as to consider three-dimensional perturbations (e.g. Yecko & Zaleski 2005). In the absence of appreciable gravitational effects, the normal-velocity eigenfunction in each fluid ϕ_j is governed by

$$\left[(U_j k_x - \omega)\left(\frac{\mathrm{d}^2}{\mathrm{d}y^2} - k_x^2 - k_z^2\right) - \frac{\mathrm{d}^2 U_j}{\mathrm{d}y^2} k_x + \mathrm{i}\nu_j \left(\frac{\mathrm{d}^2}{\mathrm{d}y^2} - k_x^2 - k_z^2\right)^2\right] \phi_j = 0, \quad (4.1)$$

where $j = \{T, B\}$ denotes the top and bottom fluids respectively. At the interface of the two fluids, all three velocity and stress components must be continuous. The interface conditions are, therefore,

$$\begin{gathered} -\mathrm{i}\omega f + \mathrm{i}k_x U f = \phi_T, \\ \phi_T = \phi_B, \end{gathered} \quad (4.2)$$

$$\begin{gathered} k_x(\phi d_y U)_T - (k_x U - \omega) d_y \phi_T = k_x(\phi d_y U)_B - (k_x U - \omega) d_y \phi_B, \\ \left(d_y^2 + k^2\right)(\mu_T \phi_T - \mu_B \phi_B) = \mathrm{i}k_x \left(\mu_T d_y^2 U_T - \mu_B d_y^2 U_B\right) f, \\ \rho_T \left(-\omega d_y \phi + k_x (U d_y \phi - \phi d_y U) + \mathrm{i}\nu \left(d_y^3 \phi - 3k^2 d_y \phi\right)\right)_T \\ -\rho_B \left(-\omega d_y \phi + k_x (U d_y \phi - \phi d_y U) + \mathrm{i}\nu \left(d_y^3 \phi - 3k^2 d_y \phi\right)\right)_B = -\mathrm{i}\sigma k^4 f, \end{gathered} \quad (4.3)$$

where σ is the surface tension and f is the interface deformation.

Similar to the single-fluid problem, the continuous spectrum is obtained from the free-stream behaviour of the O-S equation. Therefore, the dispersion relation retains

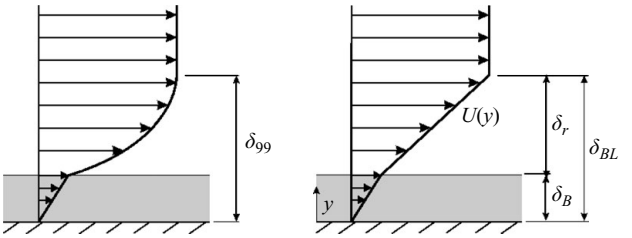

FIGURE 12. Schematic of the two-fluid mean velocity profile.

the same form,

$$-k_y^2 = k_x^2 + k_z^2 + \mathrm{i}\frac{k_x}{\nu_T}(U_\infty - \omega/k_x).$$

Note, however, that the temporal decay rate of the eigenvalue is determined solely by the viscosity of the top fluid ν_T:

$$\omega = k_x U_\infty - \mathrm{i}\nu_T\left(k_x^2 + k_z^2 + k_y^2\right), \tag{4.4}$$

4.1. *The mean flow*

A schematic of the two-fluid boundary-layer profiles used in this study is shown in figure 12. The Blasius-like mean flow profile is obtained by solving the two-fluid boundary-layer equations in an approach similar to that of Nelson, Alving & Joseph (1995). In boundary-layer coordinates, the mean-flow satisfies

$$F\partial_\eta^2 F + \nu_j \partial_\eta^3 F - \xi\left(\partial_\eta F\frac{\partial\partial_\eta F}{\partial\xi} - \partial_\eta^2 F\frac{\partial F}{\partial\xi}\right) = 0, \tag{4.5}$$

where $\xi = (U_\infty x/2\nu_T)^{1/2}$; $\eta = y(U_\infty/2\nu_T x)^{1/2}$; and $F = \Psi/(2\nu_T x U_\infty)^{1/2}$ with Ψ as the streamfunction. The interface height η^* is governed by the standard kinematic condition

$$\frac{\partial\eta^*}{\partial\xi} = \frac{1}{\xi}\left(\frac{V}{U} - \eta^*\right), \tag{4.6}$$

where U and V are the mean streamwise and wall-normal velocities at the interface respectively. Velocity and stress continuity are enforced at $\eta = \eta^*$, according to

$$[F] = 0; \quad [\partial_\eta F] = 0; \quad \left[\mu\partial_\eta^2 F\right] = 0,$$

where [.] denotes the change across the interface, $(.)_T - (.)_B$. In addition, $F(\xi, \eta)$ must satisfy the boundary conditions

$$F(\xi, 0) = 0, \quad \partial_\eta F(\xi, 0) = 0, \quad \lim_{\eta\to\infty}\partial_\eta F(\xi, \eta) = 1.$$

Equation (4.5) and the associated boundary and interface conditions are solved according to the approach described in Schlichting (1987, pp. 187–191). The iterative procedure ensures convergence of the interface height and velocity profiles at every downstream location, ξ. The solution at large ξ agrees with the asymptotic behaviour described in Nelson *et al.* (1995) and provides the mean profile for the numerical evaluation of the continuous-spectrum modes.

The piecewise linear approximation to the mean profile, which is used in the analytical derivations, is defined according to

$$\left.\begin{array}{ll} U(y) = \tau_B y, & 0 < y < \delta_B, \\ U(y) = \tau_B \delta_B + \tau_T (y - \delta_B), & \delta_B < y < \delta_{BL}, \\ U(y) = U_\infty, & y > \delta_{BL}, \end{array}\right\} \tag{4.7}$$

where

$$\delta_{BL} = \delta_{SF} + \delta_B \left(1 - \frac{\mu_T}{\mu_B}\right),$$
$$\tau_T = \frac{U_\infty}{\delta_T + \dfrac{\mu_T}{\mu_B}\delta_B} = \frac{U_\infty}{\delta_{SF}},$$
$$\tau_B = \frac{\mu_T \tau_T}{\mu_B}.$$

The single-fluid boundary-layer thickness δ_{SF} is the unit length scale, and the film thickness δ_B is a parameter. As the viscosity ratio $\mu_{BT} \equiv \mu_B/\mu_T \to \infty$, the shear in the bottom fluid vanishes, $\tau_B \to 0$. Therefore the shear predominantly resides in the top fluid, and the lower film mimics a solid wall. Conversely, as the viscosity ratio is reduced, the shear increases in the lower layer. For $\mu_{BT} < \delta_B/\delta_{SF}$, the shear is entirely limited to the wall film ($\delta_T = 0$, $\tau_T = 0$ and $\tau_B = U_\infty/\delta_B$).

4.2. *Analytical solution for piecewise linear profile*

An exact expression for the eigenfunction of the piecewise linear mean profile is sought. Similar to the single-fluid problem, an equation for ψ is derived for each layer of the mean flow:

$$\left.\begin{array}{ll} d_Y^2 \psi_{FS} + k_y^2 \psi_{FS} = 0, & Y \geqslant 0, \\ d_Y^2 \psi_T + k_y^2 \psi_T - \dfrac{\mathrm{i} k_x \tau_T}{\nu_T} Y \psi_T = 0, & 0 \geqslant Y \geqslant -\delta_T, \\ \nu_B d_Y^2 \psi_B + \left[\nu_T \left(k_x^2 + k_y^2 + k_z^2\right) - \nu_B \left(k_x^2 + k_z^2\right)\right] \psi_B & \\ + i k_x \left(\tau_T \delta_T - \tau_B \left(Y + \delta_T\right)\right) \psi_B = 0, & -\delta_T \geqslant Y \geqslant -\delta_{BL}. \end{array}\right\} \tag{4.8}$$

It is important to note that the viscosity of the top fluid, ν_T, appears in the vorticity equation of the bottom fluid because the temporal decay rate of the continuous mode is determined by the free-stream behaviour. As a result, the mode shape in the bottom fluid is expected to depend on the viscosity ratio, even in the absence of density stratification and surface tension, which only appear in the interface stress conditions.

The eigenmodes in the free stream, $Y > 0$, and in the outer boundary layer, $-\delta_T < Y < 0$, retain the same functional form as in the single-fluid problem (2.9)–(2.12). In the lower film, $-\delta_T \geqslant Y \geqslant -\delta_{BL}$, the solution for ψ_B and ϕ_B are, respectively,

$$\psi_B = C_9 \mathrm{Ai}[\mathscr{X}(Y)] + C_{10} \mathrm{Bi}[\mathscr{X}(Y)], \tag{4.9}$$

$$\begin{aligned} \phi_B = {} & \frac{\exp(-kY)}{2k} \int_{-\delta_{BL}}^{Y} \exp(ks)(C_9 \mathrm{Ai}[\mathscr{X}(s)] + C_{10} \mathrm{Bi}[\mathscr{X}(s)])\, \mathrm{d}s \\ & + \frac{\exp(kY)}{2k} \int_{Y}^{-\delta_T} \exp(ks)(C_9 \mathrm{Ai}[\mathscr{X}(s)] + C_{10} \mathrm{Bi}[\mathscr{X}(s)])\, \mathrm{d}s \\ & + C_{11} \exp(-kY) + C_{12} \exp(kY), \end{aligned} \tag{4.10}$$

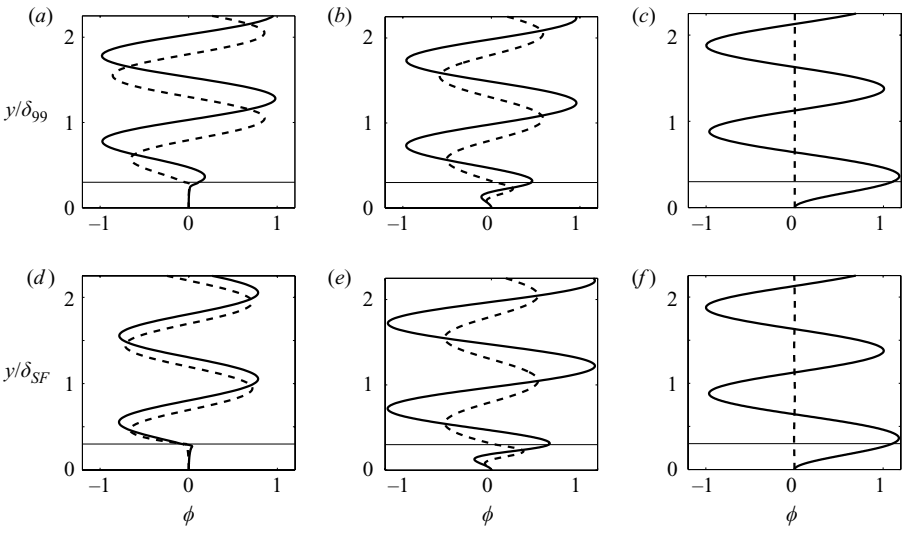

FIGURE 13. Example of continuous-mode shape for two-fluid boundary layer (top figures) and piecewise linear profile (bottom figures) in three different regimes: (*a*), (*d*) convective shear-sheltering regime $k_x Re_T = 4000\pi$, $k_y = 2\pi$, $k_z = \pi$, $\delta_B = 0.3$, $\mu_{BT} = 0.1$; (*b*), (*e*) convective–diffusive regime $k_x Re_T = 50\pi$, $k_y = 2\pi$, $k_z = \pi$, $\delta_B = 0.3$, $\mu_{BT} = 0.3$; (*c*), (*f*) diffusive regime $k_x Re_T = \pi/100$, $k_y = 2\pi$, $k_z = \pi$, $\delta_B = 0.3$, $\mu_{BT} = 0.75$; ———, real component; – – –, imaginary component.

where

$$\mathscr{X}(Y) = \exp(\mathrm{i}5\pi/6)\left(\frac{k_x\tau_B}{\nu_B}\right)^{1/3}\left(Y + \frac{\mathrm{i}\gamma\nu_B}{k_x\tau_B}\right)$$

and

$$\gamma = \frac{\nu_T k_y^2}{\nu_B} + \left(\frac{\nu_T}{\nu_B} - 1\right)(k_x^2 + k_z^2) + \frac{\mathrm{i}k_x\delta_T}{\nu_B}(\tau_T - \tau_B).$$

The constants C_1 through C_{12} are selected such that the solution satisfies the boundedness condition in the free stream, no slip at the wall and the interface conditions (4.3). Analytical expressions for the constants are too complex and are not provided. Instead, the constants are evaluated by numerical solution of the system of equations representing the boundary conditions.

An example of the two-fluid eigenfunctions, for both piecewise linear and two-fluid boundary-layer mean flow profiles, is shown in figure 13. Properties of the top fluid were chosen to ensure that the disturbance penetrates the outer shear and reaches the interface. Based on the outer flow, the eigenfunctions therefore belong to the diffusive regime, $k_x\tau_T\delta_{SF} \ll \nu_T k_y^2$. The three viscosity ratios shown in figure 13 reflect three asymptotic limits of the eigenfunction in the wall film. These limits bear resemblance to the asymptotic regimes of single-fluid boundary layers and can be determined from the ratio of convective and diffusive terms in (4.8):

(*a*) the convective, shear-sheltered regime, $k_x\tau_B\delta_B \gg \nu_T k_y^2 + (\nu_T - \nu_B)(k_x^2 + k_z^2)$;

(*b*) the diffusive regime, $k_x(\tau_T\delta_T + \tau_B\delta_B) \ll \nu_T k_y^2 + (\nu_T - \nu_B)(k_x^2 + k_z^2)$; and

(*c*) the convective–diffusive regime, $k_x\tau_B\delta_B \approx \nu_T k_y^2 + (\nu_T - \nu_B)(k_x^2 + k_z^2)$.

In order to realize conditions (*a*) and (*c*) for the shear-sheltered and convective–diffusive regimes, respectively, the viscosity of the bottom fluid must be much smaller than that of the top fluid, $\nu_B \ll \nu_T$. As a result, the shear can be assumed to be

restricted to the bottom layer. In the shear-sheltered regime, where viscosity is not significant, the two-fluid eigenfunctions are expected to bear resemblance to the single-fluid problem. However, in the other two limits, where viscous effects are appreciable, the behaviour of the two-fluid eigenfunctions is likely to be affected. Indeed, it is shown that eigenfunctions become dependent on the viscosity ratio and not the viscosity of the bottom fluid per se.

5. Asymptotic solutions in the two-fluid boundary layer

5.1. *The convective shear-sheltered regime*

Our investigation of the convective–sheltered regime assumes an oscillatory solution in the top fluid, and the shear is restricted to the bottom layer. Therefore, the following simplifications are adopted: $\tau_T = 0$, $\delta_T = 0$, $\delta_B = \delta_{BL}$ and $\tau_B = U_\infty/\delta_{BL}$. In this limit, the vorticity equation (4.8) reduces to

$$\epsilon_s \nu_B d_y^2 \psi_B + \left(\nu_T \left(k_x^2 + k_y^2 + k_z^2\right) - \nu_B \left(k_x^2 + k_z^2\right)\right)\left(\epsilon_s - \frac{\mathrm{i}Y}{\delta_B}\right)\psi_B = 0,$$

where

$$\epsilon_s \equiv \frac{\nu_T\left(k_x^2 + k_y^2 + k_z^2\right) - \nu_B\left(k_x^2 + k_z^2\right)}{k_x \tau_B \delta_{BL}} \ll 1.$$

A series expansion, $\psi_B = \epsilon_s^0 \psi_{B0} + \epsilon_s^1 \psi_{B1} + \epsilon_s^2 \psi_{B2} + \cdots$, yields trivial solutions for all powers of ϵ_s. This solution is only valid in the bulk of the lower fluid.

Similar to the single-fluid boundary layer, an edge layer exists, but is near the two-fluid interface. The solution in the edge layer satisfies the interfacial conditions and asymptotically matches the trivial solution in the bulk of the lower fluid. The vorticity equation is expressed in terms of the edge coordinate, $Y_e \equiv Y/\delta_e$, and the dominant balance yields an edge-layer thickness, $\delta_e \sim O\left(\nu_B/k_x\tau_B\right)^{1/3}$. The leading-order behaviour of the eigenfunction, ψ_{B_e}, is given according to:

$$\psi_{B_e} = C_{e_1}\mathrm{Ai}[\exp(\mathrm{i}5\pi/6)Y_e] + C_{e_2}\mathrm{Bi}[\exp(\mathrm{i}5\pi/6)Y_e]. \tag{5.1}$$

Since ψ_{B_e} must match the trivial solution in the limit $Y_e \to \infty$, the constant C_{e_2} must be identically zero and, as a result, $\psi_{B_e} = C_{e_1}\mathrm{Ai}[\exp(\mathrm{i}5\pi/6)Y_e]$.

A wall layer also exists in the vicinity of the solid boundary in order to satisfy the no-slip and no-penetration conditions. The vorticity equation is expressed in terms of the wall coordinate, $Y_w \equiv (\delta_{BL} + Y)/\delta_w$. The dominant balance yields a wall-layer thickness $\delta_w \sim O\left(\sqrt{\nu_B/k_x\tau_B\delta_{BL}}\right)$, and the following leading-order solution for ψ_{B_w} is obtained:

$$\psi_{B\,w}(Y_w) = C'_{w_1}\exp\left(\frac{1}{\sqrt{2}}(1-\mathrm{i})Y_w\right) + C'_{w_2}\exp\left(-\frac{1}{\sqrt{2}}(1-\mathrm{i})Y_w\right). \tag{5.2}$$

Since the solution in the wall layer must match the trivial solution in the bulk of the bottom fluid, $\psi_{B_w}(Y_w \to \infty) = 0$, and therefore $C'_{w_1} = 0$.

A uniformly valid approximation of the eigenfunction is sought in the bottom fluid, $Y \in [-\delta_{BL}, 0]$. The solution combines the edge, bulk and wall-layer solutions. To the leading order, the vorticity eigenfunctions is given according to:

$$\psi_B = C_{e_1}\mathrm{Ai}[z(Y)] + C'_{w_2}\exp(-\zeta(\delta_{BL} + Y)), \tag{5.3}$$

where $z(Y) = \exp(\mathrm{i}5\pi/6)(k_x\tau_B/\nu_B)^{1/3}Y$ and $\zeta = (1-\mathrm{i})/\sqrt{2}\delta_w$. The corresponding vertical-velocity eigenfunction in the bottom fluid is therefore

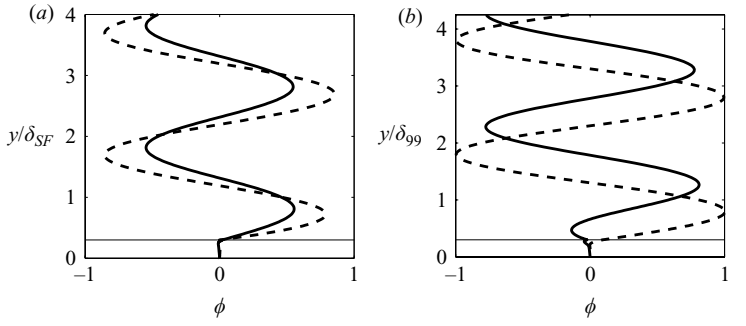

FIGURE 14. Continuous-mode shape in convective shear-sheltering regime. (*a*) Eigenfunction for a piecewise linear profile and (*b*) eigenfunction for a two-fluid boundary layer; ———, real component; – – –, imaginary component; $k_x Re_T = 500\pi$, $k_y = \pi$, $k_z = \pi$, $\delta_B = 0.3$, $\mu_{BT} = 0.1$.

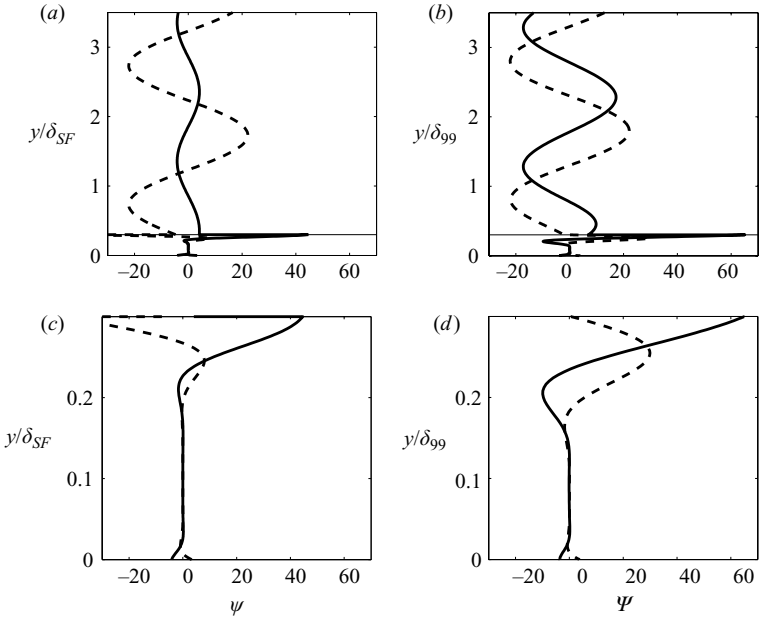

FIGURE 15. Spanwise vorticity in convective shear-sheltering regime with three-layered structure. (*a*), (*c*) Eigenfunction for a piecewise linear profile and (*b*), (*d*) eigenfunction for a two-fluid boundary layer; ———, real component; – – –, imaginary component; $k_x Re_T = 500\pi$, $k_y = \pi$, $k_z = \pi$, $\delta_B = 0.3$, $\mu_{BT} = 0.1$.

$$\phi_B = \frac{C_{e_1}}{2k}\left[\exp(-kY)\int_{-\delta_{BL}}^{Y}\exp(ks)\mathrm{Ai}[z(s)]\,\mathrm{d}s + \exp(kY)\int_{Y}^{0}\exp(ks)\mathrm{Ai}[z(s)]\,\mathrm{d}s\right] + C_{w_2}\exp(-\zeta(\delta_{BL}+Y)) + C_9\exp(-kY) + C_{10}\exp(kY). \quad (5.4)$$

An example of a vertical-velocity eigenfunction, ϕ, which penetrates the top fluid, but is sheltered by the shear in the bottom layer is shown in figure 14. The behaviour is consistent among the piecewise linear and two-fluid boundary-layer eigenfunctions. Figure 15 shows the vorticity of the same mode, ψ. In the lower fluid, there exists a three-layer structure similar to that observed in the single-fluid boundary layer.

A noticeable difference between the two-fluid and the previously derived single-fluid eigenfunctions is the sharp discontinuity in ψ at the interface. This discontinuity arises due to the interface conditions, even when both fluids have equal densities

and surface tension is ignored. The normal-velocity eigenfunction shows that $\phi \to 0$ at the interface, which implies that the interface displacement is negligible. The interface, therefore, resembles a rigid membrane which prevents free-stream vortical disturbances from entering the bottom fluid.

5.2. *The diffusive regime*

In the diffusive regime, viscous effects dominate the convective term in the vorticity equation (4.8) of the bottom fluid. Therefore, the small parameter ϵ_d is defined as the ratio of the convective to viscous terms,

$$\epsilon_d \equiv \frac{k_x(\tau_T \delta_T + \tau_B \delta_B)}{\nu_T k_y^2 + (\nu_T - \nu_B)(k_x^2 + k_z^2)} \ll 1.$$

In terms of ϵ_d, the vorticity equation (4.8) can be expressed as

$$\frac{\nu_B}{\nu_T\left(k_x^2 + k_y^2 + k_z^2\right) - \nu_B\left(k_x^2 + k_z^2\right)} d_Y^2 \psi_B + \psi_B + \mathrm{i}\epsilon_d \frac{\tau_T \delta_T - \tau_B(Y + \delta_T)}{\tau_T \delta_T + \tau_B \delta_B} \psi_B = 0.$$

A series solution of ψ in powers of ϵ_d is assumed. The leading-order term in the expansion is governed by the following equation:

$$\frac{\nu_B}{\nu_T\left(k_x^2 + k_y^2 + k_z^2\right) - \nu_B\left(k_x^2 + k_z^2\right)} d_Y^2 \psi_B + \psi_B = 0,$$

and the leading-order solution is therefore

$$\psi_B = C_9' \exp(-\mathrm{i}\kappa_d Y) + C_{10}' \exp(\mathrm{i}\kappa_d Y),$$
$$\phi_B = C_9 \exp(-\mathrm{i}\kappa_d Y) + C_{10} \exp(\mathrm{i}\kappa_d Y) + C_{11} \exp(-kY) + C_{12} \exp(kY),$$

where $\kappa_d = \sqrt{(\nu_T/\nu_B)(k_x^2 + k_y^2 + k_z^2) - (k_x^2 + k_z^2)}$. The constants C_1 through C_{12} are obtained by constructing a system of equations representing the wall, free-stream and interface conditions (4.3) and solving it numerically.

In contrast to the single-fluid eigenfunctions, the two-fluid solution predicts an effective wall-normal wavenumber κ_d, which differs from the free-stream value k_y. The definition of κ_d indicates that the solution changes from oscillatory to exponential behaviour at a critical viscosity ratio, $(\nu_B/\nu_T)_c = (k_x^2 + k_y^2 + k_z^2)/(k_x^2 + k_z^2)$. For a viscosity ratio ν_B/ν_T lower than the critical value, an oscillatory solution is obtained; for ν_B/ν_T greater than the critical ratio, the solution is exponential. This change in the character of the solution is demonstrated in figure 16, where ψ is plotted at subcritical and supercritical viscosity ratios.

The change in the wall-normal wavenumber, $\kappa_d \neq k_y$, is due to a mismatch in dissipation and diffusion in the streamwise and spanwise directions: The continuous mode temporal decay rate is determined by the free-stream viscosity and is proportional to $\nu_T(k_x^2 + k_z^2)$. In the lower fluid, however, diffusion is proportional to $\nu_B(k_x^2 + k_z^2)$. The mismatch between the modal decay rate and diffusion in the bottom fluid causes the distortion of the wall-normal wavenumber; this distortion ensures that the diffusion term in the bottom fluid O-S equation maintains the correct modal decay rate, set by the free stream.

For instance, consider a bottom fluid with lower viscosity than the free stream. The streamwise and spanwise diffusions in this layer will therefore be smaller than the free-stream values. As a result, the effective wall-normal wavenumber κ_d in the bottom fluid must be greater than k_y, in order to match the free-stream prescribed modal decay rate.

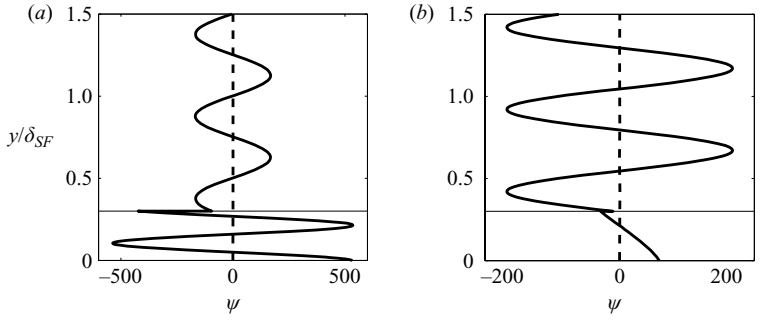

FIGURE 16. Change in nature of spanwise vorticity from oscillatory to exponential in the film at different ratios of ν_B/ν_T; ———, real component; – – –, imaginary component; $k_x Re_T = \pi/10$, $k_y = 4\pi$, $k_z = \pi$, $\delta_B = 0.3$. (*a*) $\nu_B/\nu_T = 0.2$. (*b*) $\nu_B/\nu_T = 5$.

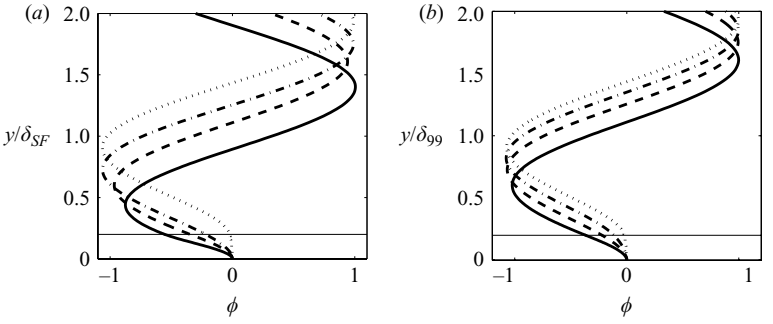

FIGURE 17. Effect of ν_{BT} on penetration of continuous modes for (*a*) piecewise linear profile and (*b*) two-fluid boundary layer; $k_x Re_T = \pi/10$, $k_y = \pi$, $k_z = \pi$, $\delta_B = 0.2$; ———, $\mu_{BT} = 0.5$; – – –, $\mu_{BT} = 1$; —·—, $\mu_{BT} = 2(\nu_{r\,crit})$; ·····, $\mu_{BT} = 10$.

The change in the wall-normal wavenumber is significant in correctly explaining penetration of vortical disturbances in two-fluid boundary layer. In the single-fluid problem, it was shown that modal penetration into the shear is proportional to $k_y^2 \nu / k_x \tau \delta$, where k_y^2 is a parameter, and low viscosity implies weak penetration, while higher viscosity enhances penetration. This dependence is not, however, preserved in the two-fluid problem. Instead, the expression for penetration must be updated to account for the modified wavenumber, $\kappa_d^2 \nu_B / k_x \tau \delta$. A reduction of ν_B, alone, would reduce penetration. However, the associated increase in κ_d causes a net increase in penetration at lower ν_B. Conversely, an increase in ν_B and the associated reduction in κ_d cause an overall reduction in penetration, opposite to the prediction for a single-fluid shear flow. These observations are confirmed in figure 17 in which the eigenfunction is plotted at various viscosity ratios; higher ν_B is shown to reduce modal penetration.

5.3. *The convective–diffusive regime*

In this regime, both the viscous and convective terms in the vorticity equation (4.8) of the bottom fluid are of the same order:

$$\nu_T \left(k_x^2 + k_y^2 + k_z^2\right) - \nu_B \left(k_x^2 + k_z^2\right) \approx k_x \tau_B \delta_{BL}.$$

If a fully penetrating solution is assumed in the outer fluid, the above condition necessitates that τ_B is sufficiently large; here the shear is assumed to be restricted to the near-wall region, and as a result, the interface is located at $Y=0$.

The asymptotic behaviour of the solution near the interface is derived by considering the limit $Y\to 0$ of the vorticity equation (4.8), which yields

$$\nu_B\frac{\mathrm{d}^2\psi^0_{Be}}{\mathrm{d}Y^2}+\left(\nu_T\left(k_x^2+k_y^2+k_z^2\right)-\nu_B\left(k_x^2+k_z^2\right)\right)\psi^0_{Be}=0,$$

The solution near the interface is therefore

$$\psi^0_{Be}=\underbrace{C_{e_1}\exp(\mathrm{i}\kappa_e Y)}_{\psi^0_{Be_1}}+\underbrace{C_{e_2}\exp(-\mathrm{i}\kappa_e Y)}_{\psi^0_{Be_2}},\tag{5.5}$$

where $\kappa_e=\sqrt{(\nu_T/\nu_B)(k_x^2+k_y^2+k_z^2)-(k_x^2+k_z^2)}$. The effect of the shear on the wall-normal decay of the eigenfunction is not captured in this expression. Therefore, similar to the analysis of the single-fluid problem, corrections to the two linearly independent solutions $\psi^0_{Be_{\{1,2\}}}$ are sought, and the final expression for the eigenfunction near the interface is given according to

$$\begin{aligned}\psi_{Be}=&\underbrace{C_{e1}\mathrm{e}^{\mathrm{i}\kappa_e Y}}_{\psi^0_{Be_1}}+\underbrace{C_{e1}\mathrm{e}^{\mathrm{i}k_e Y}\left[\frac{k_x\tau_B}{2k_e\nu_B}\left(\frac{Y^2}{2}-\frac{Y}{2\mathrm{i}\kappa_e}-\frac{1-\mathrm{e}^{-2\mathrm{i}\kappa_e Y}}{4\kappa_e^2}\right)\right]}_{\psi^1_{Be_1}}\\&+\underbrace{C_{e2}\mathrm{e}^{-\mathrm{i}\kappa_e Y}}_{\psi^0_{Be_2}}+\underbrace{C_{e2}\mathrm{e}^{-\mathrm{i}k_e Y}\left[-\frac{k_x\tau_B}{2k_e\nu_B}\left(\frac{Y^2}{2}+\frac{Y}{2\mathrm{i}\kappa_e}-\frac{1-\mathrm{e}^{2i\kappa_e Y}}{4k_e^2}\right)\right]}_{\psi^1_{Be_2}}.\end{aligned}\tag{5.6}$$

The constants C_{e1} and C_{e2} are calculated by enforcing continuity of ψ, and its gradient at $Y=0$ and are provided in § B.1 of Appendix B. The above solution in the edge layer is compared to the exact analytical expression (4.9) in figure 18, and good quantitative agreement is observed. The wall-normal oscillation due to $\psi^0_{Be_{\{1,2\}}}$ is similar to that in the diffusive regime, at the modified wall-normal wavenumber, $\kappa_e=\kappa_d$. The decay of the solution inside the bottom fluid, away from the interface, is due to the cancellation by $\psi^1_{Be_{\{1,2\}}}$, where the influence of the shear is cumulative and increases with distance from the interface.

In the vicinity of the wall, the behaviour of ψ is described by the limit $Y\to-\delta_{BL}$ of (4.8) for the bottom fluid. To the lowest order in Y, the governing equation becomes

$$\nu_B\frac{\mathrm{d}^2\psi^0_{B_w}}{\mathrm{d}Y^2}+\left(\nu_T\left(k_x^2+k_y^2+k_z^2\right)-\nu_B(k_x^2+k_z^2)+\mathrm{i}k_x\tau_B\delta_{BL}\right)\psi^0_{B_w}=0$$

and has the solution

$$\psi^0_{Bw}=\underbrace{C_{w_1}\exp(\mathrm{i}\kappa_w(Y+\delta_{BL}))}_{\psi^0_{Bw_1}}+\underbrace{C_{w_2}\exp(-\mathrm{i}\kappa_w(Y+\delta_{BL}))}_{\psi^0_{Bw_2}},\tag{5.7}$$

where

$$\kappa_w=\sqrt{\frac{\nu_T}{\nu_B}\left(k_x^2+k_y^2+k_z^2\right)-\left(k_x^2+k_z^2\right)+\mathrm{i}\frac{k_x\tau_B\delta_{BL}}{\nu_B}}.$$

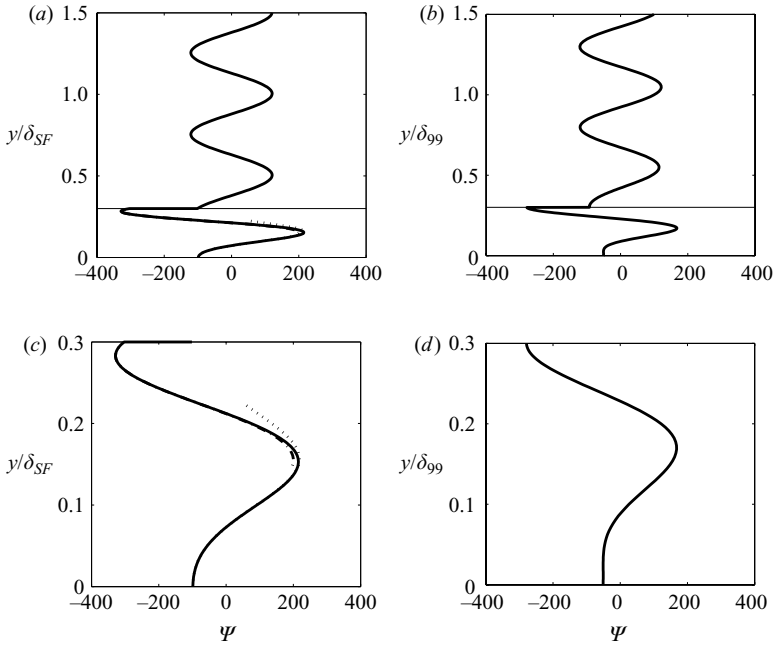

FIGURE 18. Structure of spanwise vorticity in the convective–diffusive regime, showing the edge- and wall-layer solutions for piecewise linear profile. The real part of the exact analytical solution (———), the asymptotic solution in the edge layer (—·—) and the asymptotic solution in the wall layer (·····) are compared; $k_x Re_T = 50\pi$, $k_y = 4\pi$, $k_z = \pi$, $\delta_B = 0.3$, $\mu_{BT} = 0.3$.

Correction terms to ψ^0_{Bw} are derived using a similar procedure to the edge layer, and the following near-wall solution is obtained:

$$\begin{aligned}\psi_{Bw} = {} & C_{w1}\mathrm{e}^{\mathrm{i}k_w(Y+\delta_{BL})} + C_{w2}\mathrm{e}^{-\mathrm{i}k_w(Y+\delta_{BL})} \\ & + C_{w1}\mathrm{e}^{\mathrm{i}k_w(Y+\delta_{BL})}\left[\frac{k_x\tau_B}{2k_w\nu_B}\left(\frac{(Y+\delta_{BL})^2}{2} - \frac{(Y+\delta_{BL})}{2\mathrm{i}k_w} - \frac{1-\mathrm{e}^{-2\mathrm{i}k_w(Y+\delta_{BL})}}{4k_w^2}\right)\right] \\ & + C_{w2}\mathrm{e}^{-\mathrm{i}k_w(Y+\delta_{BL})}\left[\frac{-k_x\tau_B}{2k_w\nu_B}\left(\frac{(Y+\delta_{BL})^2}{2} + \frac{(Y+\delta_{BL})}{2\mathrm{i}k_w} - \frac{1-\mathrm{e}^{2\mathrm{i}k_w(Y+\delta_{BL})}}{4k_w^2}\right)\right].\end{aligned}$$

The constants C_{w1} and C_{w2} are evaluated by imposing wall-boundary conditions on ψ and its gradient (§ B.1 of Appendix B). The wall solution accurately captures the exact solution in the near-wall region as shown in figure 18.

The complex κ_w implies that the solution is oscillatory and also decaying. The deviation of the solution from the purely oscillatory form is characteristic of the convective–diffusive regime. This deviation is due to the term $k_x\tau_B\delta_{BL}/\nu_B$, which is the cumulative effect of shear sheltering over the depth of the boundary layer as discussed in the single-fluid problem and shown in figure 18.

It was demonstrated in the viscous regime that penetration is enhanced at low ν_B due to the modified wavenumber, $\kappa_d > k_y$. A similar effect can be observed in the convective–diffusive regime: The definition of κ_w indicates that for low ν_B modal penetration is enhanced by the modified wavenumber, $\mathrm{Re}(\kappa_w) > k_y$. However, the wall-normal decay $\mathscr{I}(\kappa_w)$ is also increased for small ν_B. Therefore, it is not clear whether a lower viscosity film enhances or reduces the penetration of the vortical disturbance into the bottom fluid. Further discussion of the dependence of penetration

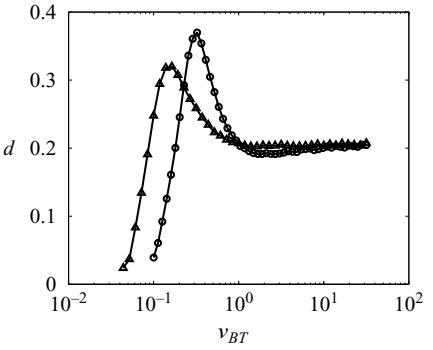

FIGURE 19. Variation of penetration depth with viscosity ratio in which $k_x Re_T = 1/100$, $k_y = \pi/4$, $k_z = \pi$; ○, $\delta_B = 0.3$; △, $\delta_B = 0.2$.

on viscosity ratio, density ratio and surface tension is therefore presented in the next section and is explained in light of the above-derived asymptotic solutions.

6. Discussion

In this paper, asymptotic solutions have been derived for the continuous-spectrum modes of single- and two-fluid boundary layers. The competition between the convective and diffusive terms in the O-S equations delineated the various possible asymptotic regimes, and a physical interpretation of shear sheltering was provided. In the single-fluid problem, it was shown that penetration of the vortical disturbance into the boundary layer was enhanced by viscosity and limited by the shear. The influence of introducing a fluid of different viscosity near the wall is complex. For instance, a low-viscosity film enhances shear sheltering and, as a result, can suppress the eigenfunction in the bottom fluid. However, another competing mechanism emerges due to viscosity stratification: an increase in the apparent wall-normal wavenumber can result in enhanced penetration of the vortical mode at low viscosity. This competition suggests an optimal viscosity ratio exists, whereby penetration of the disturbances in the two-fluid boundary layer is maximum.

The effect of viscosity ratio on penetration depth, d, for the continuous modes of the two-fluid boundary layer is shown in figure 19. Indeed an optimal viscosity ratio $\nu_{BT}^{\star} \equiv (\nu_B/\nu_T)^{\star}$ exists where d is maximum. The optimal viscosity ratio is less than unity, indicating maximum modal penetration into the shear takes place when the lower fluid is less viscous, contrary to the results from the single-fluid analysis.

In the limit $\nu_{BT} \gg 1$, the bottom fluid simulates the influence of a solid wall. As a result, the penetration d asymptotes to the single-fluid limit. A reduction in the viscosity of the lower fluid, $\nu_{BT}^{\star} < \nu_{BT} < 1$, is observed to increase penetration. Despite an expected reduction in d for lower ν_B, penetration in fact increases due the modified wavenumber, $\kappa_d > k_y$, as discussed in the diffusive regime (§ 5.2). Upon further reduction of ν_B, the convective term becomes appreciable, and the eigenfunction falls within the convective–diffusive regime (§ 5.3). Due to shear sheltering, d decays for $\nu_{BT} < \nu_{BT}^{\star}$. The influence of the shear continues to amplify for smaller ν_{BT} ratios, and the eigenfunctions transitions into the shear-sheltered regime (§ 5.1). In this limit, the

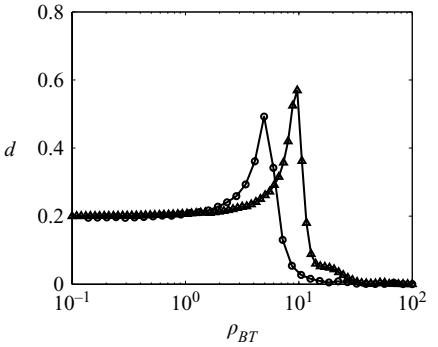

FIGURE 20. Variation of penetration depth with density ratio in which $k_x Re_T = 1/100,\ k_y = \pi/4,\ k_z = \pi,\ \mu_{BT} = 1,\ We^{-1} = 0$; ○, $\delta_B = 0.3$; △, $\delta_B = 0.2$.

vortical modes are unable to significantly perturb the interface, which resembles a stiff membrane.

6.1. *Density stratification*

In the eigenvalue problem, the density ratio appears in the normal-stress interface condition and implicitly in the O-S equation via the kinematic viscosity. In order to isolate the effect of density, it is assumed that the dynamic viscosities of the two fluids are identical, $\mu_B = \mu_T$, and surface tension is ignored. The dependence of penetration d on density ratio, $\rho_{BT} \equiv \rho_B/\rho_T$, is shown in figure 20. An optimal ratio exists and directly corresponds to the optimal $\nu^{\star}_{BT}$.

The first asymptotic limit in figure 20 is $\rho_{BT} \ll 1$. This regime corresponds to the previously considered limit of $\nu_{BT} \gg 1$ in figure 19. In that regime, it was shown that the bottom fluid acts as a highly viscous or solid surface, and as a result penetration is limited to the single-fluid behaviour.

In the limit of large density ratio, figure 20 shows that penetration d is negligible, even for low-k_x eigenfunctions which can effectively penetrate single-fluid boundary layers. Intuitively, this is not surprising, since the density of the bottom fluid is very large and expels external perturbations. An example of an eigenfunction from this limit is shown in figure 21. The amplitudes of both ψ and ϕ are significantly reduced across the interface. It is curious, however, that their wall-normal wavenumber increases.

An explanation can be provided from the O-S equation and the normal-stress condition across the interface. In order to simplify the analysis, we consider low-k_x disturbances in which shear sheltering is ineffective; any decay in the eigenfunction cannot therefore be attributed to the shear. In addition, we assume $1/\rho_{BT} = \epsilon_R$, and therefore the equation for ψ reduces to

$$\frac{\epsilon_R}{\delta_R^2}\frac{\mathrm{d}^2\psi_B}{\mathrm{d}Y_R^2} + \left(\left(k_x^2 + k_y^2 + k_z^2\right) - \epsilon_R\left(k_x^2 + k_z^2\right)\right)\psi_B = 0,$$

where $Y_R = Y/\delta_R$. From the balance of the dominant terms, $\delta_R \sim O(\epsilon_R/k_x^2 + k_y^2 + k_z^2)^{1/2}$, and the solution to the governing equation is therefore

$$\psi_B = C_1 \exp(-\mathrm{i}\kappa_R Y) + C_2 \exp(\mathrm{i}\kappa_R Y), \tag{6.1}$$

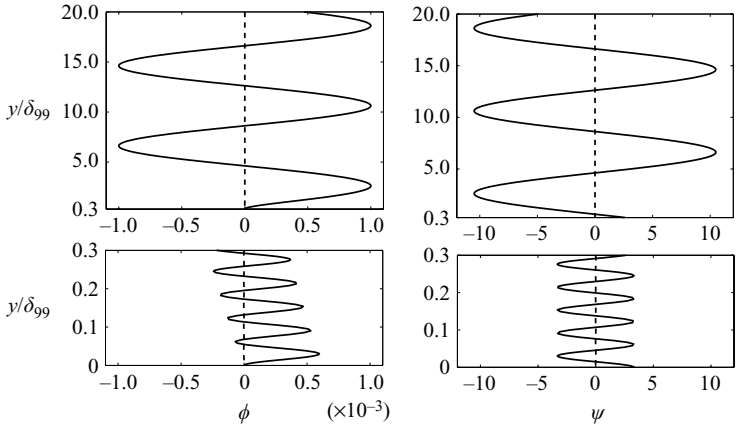

FIGURE 21. High-frequency oscillations in mode shape for an extremely dense film; ——, real component; – – –, imaginary component; $k_x Re_T = 1/100$, $k_y = \pi/4$, $k_z = \pi$, $\delta_B = 0.3$, $\rho_{BT} = 1000$. Note ϕ is plotted on separate scales in the top and bottom fluids.

where $\kappa_R = \sqrt{(1/\epsilon_R)(k_x^2 + k_y^2 + k_z^2)}$. The solution exhibits an oscillation at the modified wavenumber, $\kappa_R \gg k_y$, consistent with figure 21. This solution, per se, does not explain the reduction of the amplitude of the eigenfunction across the interface — an issue addressed by considering the normal-stress condition.

In the limit of $1/\rho_{BT} = \epsilon_R$, the interface stress condition (4.3) is expressed in the form

$$\left(k_x^2 + k_y^2 + k_z^2\right) d_Y \phi_T + \epsilon_R \left(d_Y^3 \phi_T - d_Y^3 \phi_B\right) = 0.$$

A comparison of the free-stream behaviour of the eigenfunction and the solution in the bottom fluid (6.1) shows that $(d_Y^3 \phi_T \sim k_y^3 \phi_T) \ll (d_Y^3 \phi_B \sim \kappa_R^3 \phi_B)$. Therefore, the normal-stress condition can be simplified:

$$\left(k_x^2 + k_y^2 + k_z^2\right) d_Y \phi_T = \epsilon_R d_Y^3 \phi_B.$$

Assuming oscillatory solution in both the top and bottom fluids, the interface condition indicates that

$$\phi_B \sim \sqrt{\frac{\epsilon_R k_y^2}{k_x^2 + k_y^2 + k_z^2}} \phi_T,$$

which explains the reduction in the amplitude of the eigenfunction observed in figure 21.

6.2. *Surface tension*

Surface tension appears in the normal-stress interface condition only. In order to isolate its effect, it is assumed that the density and viscosity of the two fluid are identical. Therefore, the normal-stress boundary condition reduces to

$$d_Y^3 \phi_T - d_Y^3 \phi_B = -\left(\frac{\sigma}{\nu_T}\right) k^4 f. \tag{6.2}$$

The stress condition hints at the dependence of mode shapes on surface tension; the eigenfunction is fully defined by the solution to the O-S equation. For low surface

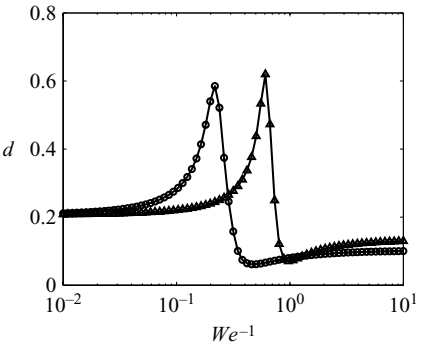

FIGURE 22. Variation of penetration depth with surface tension in which $k_x Re_T = 1/100$, $k_y = \pi/4$, $k_z = \pi$, $\mu_{BT} = 1$, $\rho_{BT} = 1$; ○, $\delta_B = 0.3$; △, $\delta_B = 0.2$.

tension, $\sigma \sim \epsilon_\sigma$, the stress condition recovers the single-fluid behaviour in which $d_y^3\phi$ is continuous across a 'virtual' interface. In the opposite limit of large $\sigma \to \infty$, the interface deformation must tend to zero, $f \to 0$, in order to maintain boundedness in the normal-stress condition. Since the interface displacement is trivial, the normal velocity at the interface also tends to zero. This is consistent with physical intuition: at high surface tension, the interface is expected to resemble a rigid membrane which prevents any perturbation from the upper layer to penetrate into the lower fluid and vice versa.

The limits of low and high surface tensions are observed in figure 22, where penetration d is plotted as a function of inverse Weber number. At low surface tension, the single-fluid limit is recovered and is common among the two curves which correspond to two different film thicknesses. In the opposite limit, $We^{-1} \gg 1$, penetration is reduced below the single-fluid limit. In this regime, the bottom fluid is shielded from the external vortical perturbation, and therefore, the asymptotic value of d is dependent on the film thickness. For the intermediate values of We^{-1}, a maximum is observed in the penetration depth. This observation suggests that elasticity of the interface due to surface tension constructively enforces the penetration of the free-stream vortical disturbance into the shear.

7. Conclusion

The penetration of free-stream vortical disturbances into single- and two-fluid boundary layers was examined using analytical and asymptotic solutions of the O-S equation. Three asymptotic regimes were identified, which are determined by the ratio of the diffusive to the convective terms in the vorticity equation. In the shear-sheltered regime, the oscillatory free-stream disturbances are simply convected by the outer flow and are exponentially decaying at the edge of the boundary layer. In the viscous regime, the oscillatory solution persists towards the wall. In the intermediate regime, both wall-normal diffusion and the accumulative effect of shear sheltering with increased depth causes a gradual decay of the oscillatory eigenfunction. The analytical solutions were complemented by a physical interpretation of shear sheltering, which contrasts low- and high-frequency modes and their ability to penetrate the shear.

The analysis of the two-fluid O-S equation was guided by the findings of the single-fluid problem. The extent of penetration of vortical modes into the lower film was

shown to depend *not* on the viscosity of the film per se but on the viscosity ratio for the following reason: The decay rate of the continuous modes is determined by the free-stream viscosity which does not match that of the lower fluid. A modified wall-normal wavenumber, which is proportional to the viscosity ratio, therefore emerges and ensures that diffusion in the bottom layer matches the dissipation rate set by the free stream. Lower viscosity films caused the modified wavenumber, κ_d, to increase which in turn led to deeper penetration. This is contrary to the single-fluid boundary layer in which lower viscosities enhance shear sheltering and hence reduce penetration of the continuous modes.

Appendix A. Coefficient of the single-fluid eigenfunctions

A.1. *Analytical solution*

The exact analytical solution for ϕ is

$$\begin{aligned}
\phi &= C_1\exp(-\mathrm{i}k_y Y) + C_2\exp(\mathrm{i}k_y Y) + C_3\exp(-kY), \quad Y > 0,\\
\phi &= C_7\exp(-kY) + C_8\exp(kY) + \exp(-kY)\\
&\quad\times \int_{-\delta_{BL}}^{Y} \exp(ks)(C_5\mathrm{Ai}[\mathscr{Z}(s)] + C_6\mathrm{Bi}[\mathscr{Z}(s)])\,\mathrm{d}s + \exp(kY)\\
&\quad\times \int_{Y}^{0} \exp(-ks)(C_5\mathrm{Ai}[\mathscr{Z}(s)] + C_6\mathrm{Bi}[\mathscr{Z}(s)])\,\mathrm{d}s, \quad -\delta_{BL} < Y < 0,
\end{aligned}$$

and the coefficients are

$$\left.\begin{aligned}
C_5 &= \frac{C_3}{\dfrac{\mathrm{Ai}[\mathscr{Z}(0)]}{k^2+k_y^2} + A^- - A^+ - \lambda\left(\dfrac{\mathrm{Bi}[\mathscr{Z}(0)]}{k^2+k_y^2} + B^- - B^+\right)},\\
C_6 &= \lambda C_5\\
C_1 &= \frac{1}{2}\left[\frac{k}{\mathrm{i}k_y}(C_5(A^- + A^+) + C_6(B^- + B^+)) + \frac{k_x\tau(C_5\mathrm{Ai}[\mathscr{Z}(0)] + C_6\mathrm{Bi}[\mathscr{Z}(0)])}{\nu k_y\left(k^2+k_y^2\right)^2}\right.\\
&\quad\left. - \frac{C_5\mathrm{Ai}[\mathscr{Z}(0)] + C_6\mathrm{Bi}[\mathscr{Z}(0)]}{k^2+k_y^2} - C_3\left(\frac{k}{\mathrm{i}k_y} + \frac{k_x\tau}{\nu k_y\left(k^2+k_y^2\right)}\right)\right],\\
C_2 &= \frac{-1}{2}\left[\frac{k}{\mathrm{i}k_y}(C_5(A^- + A^+) + C_6(B^- + B^+)) + \frac{k_x\tau(C_5\mathrm{Ai}[\mathscr{Z}(0)] + C_6\mathrm{Bi}[\mathscr{Z}(0)])}{\nu k_y\left(k^2+k_y^2\right)^2}\right.\\
&\quad\left. + \frac{C_5\mathrm{Ai}[\mathscr{Z}(0)] + C_6\mathrm{Bi}[\mathscr{Z}(0)]}{k^2+k_y^2} - C_3\left(\frac{k}{\mathrm{i}k_y} + \frac{k_x\tau}{\nu k_y\left(k^2+k_y^2\right)}\right)\right],\\
C_7 &= 0,\\
C_8 &= -(C_5A^+ + C_6B^+),
\end{aligned}\right\} \tag{A 1}$$

where

$$A^{\pm} = \frac{1}{2k}\int_{-\delta_{BL}}^{0} \exp(\pm ks)\mathrm{Ai}[\mathscr{Z}(s)]ds, \quad B^{\pm} = \frac{1}{2k}\int_{-\delta_{BL}}^{0} \exp(\pm ks)\mathrm{Bi}[\mathscr{Z}(s)]\,\mathrm{d}s,$$

$$\lambda = \frac{-2kA^+ + \dfrac{k\mathrm{Ai}[\mathscr{Z}(0)] - \mathrm{Ai}'[\mathscr{Z}(0)]\mathscr{Z}'(0)}{k^2+k_y^2} - \dfrac{\left(3k^2+k_y^2\right)k_x\tau}{\mathrm{i}\nu\left(k^2+k_y^2\right)^2}(A^- - A^+)}{2kB^+ + \dfrac{-k\mathrm{Bi}[\mathscr{Z}(0)] - \mathrm{Bi}'[\mathscr{Z}(0)]\mathscr{Z}'(0)}{k^2+k_y^2} + \dfrac{\left(3k^2+k_y^2\right)k_x\tau}{\mathrm{i}\nu\left(k^2+k_y^2\right)^2}(B^- - B^+)}$$

and $\mathscr{Z}(Y) = \exp(\mathrm{i}5\pi/6)(k_x\tau/\nu)^{1/3}(Y - \mathrm{i}k_y^2\nu/k_x\tau)$.

A.2. *The convective shear-sheltered regime*

The solution for ϕ is

$$\phi = C_1\exp(-\mathrm{i}k_yY) + C_2\exp(\mathrm{i}k_yY) + C_3\exp(-kY),\ \ Y > 0,$$

$$\phi = C_5\exp(-kY) + C_6\exp(kY) + C_{w_2}(-\zeta(\delta_{BL}+Y)) + C_{e_1}\left[\exp(-kY)\int_{-\delta_{BL}}^{Y}\exp(-ks)\mathrm{Ai}[\varsigma(s)]\mathrm{d}s + \exp(kY)\int_{Y}^{0}\exp(-ks)\mathrm{Ai}[\varsigma(s)]\,\mathrm{d}s\right],\quad -\delta_{BL} < Y < 0,$$

and the coefficients are

$$\left.\begin{aligned}
C_{e_1} &= C_1\left[\frac{\mathrm{Ai}[0]}{k^2+k_y^2} + A^- - A^+ + \lambda\left(-\frac{k_y^2+\zeta^2}{k^2+k_y^2}\exp(\zeta\delta_{BL}) + \frac{k-\zeta}{2k}\exp(-k\delta_{BL}) - \frac{k+\zeta}{2k}\exp(k\delta_{BL})\right)\right]^{-1},\\
C_{w_2} &= \lambda C_{e_1},\\
C_1 &= \frac{1}{2}\left(-C_{e_1}\frac{\mathrm{Ai}[\varsigma(0)] + \mathrm{Ai}'[\varsigma(0)]\dfrac{\varsigma'}{\mathrm{i}k_y}}{k^2+k_y^2} + C_{w_2}\left(1+\frac{\zeta}{\mathrm{i}k_y}\right)\frac{k^2-\zeta^2}{k^2+\zeta^2}\exp(\zeta\delta_{BL}),\right.\\
&\quad \left. -\frac{2k^2k_x\tau}{\nu k_y\left(k^2+k_y^2\right)^2}\left(C_{w_2}\frac{k^2-\zeta^2}{k^2+\zeta^2}\exp(\zeta\delta_{BL}) - C_{e_1}\frac{\mathrm{Ai}[0]}{k^2+k_y^2} + C_3\right)\right),\\
C_2 &= \frac{1}{2}\left(-C_{e_1}\frac{\mathrm{Ai}[\varsigma(0)] - \mathrm{Ai}'[\varsigma(0)]\dfrac{\varsigma'}{\mathrm{i}k_y}}{k^2+k_y^2} + C_{w_2}\left(1+\frac{\zeta}{\mathrm{i}k_y}\right)\frac{k^2-\zeta^2}{k^2+\zeta^2}\exp(\zeta\delta_{BL})\right.\\
&\quad \left. +\frac{2k^2k_x\tau}{\nu k_y\left(k^2+k_y^2\right)^2}\left(C_{w_2}\frac{k^2-\zeta^2}{k^2+\zeta^2}\exp(\zeta\delta_{BL}) - C_{e_1}\frac{\mathrm{Ai}[0]}{k^2+k_y^2} + C_3\right)\right),\\
C_5 &= -\frac{k+\zeta}{2k}C_{w_2}\exp(k\delta_{BL}),\\
C_6 &= -C_{e_1}A^+ - \frac{k-\zeta}{2k}C_{w_2}\exp(-k\delta_{BL}),
\end{aligned}\right\} \quad (A\,2)$$

where

$$A^{\pm} = \frac{1}{2k}\int_{-\delta_{BL}}^{0}\exp\,(\pm ks)\mathrm{Ai}[\varsigma(s)]\,\mathrm{d}s,$$

$$\lambda = \frac{\dfrac{1}{k^2+k_y^2}(k\mathrm{Ai}[0]-\mathrm{Ai}'[\varsigma(0)]\varsigma'[0]) - 2kA^+ + \dfrac{k_x\tau(k_y^2+3k^2)}{\mathrm{i}\nu(k^2+k_y^2)^2}(A^- - A^+)}{(k-\zeta)\left(\exp(-k\delta_{BL}) - \dfrac{k_y^2+\zeta^2}{k^2+k_y^2}\exp(\zeta\delta_{BL})\right) - \dfrac{k_x\tau(k_y^2+3k^2)}{\mathrm{i}\nu(k^2+k_y^2)^2}\left(\exp(\zeta\delta_{BL}) - \dfrac{k-\zeta}{2k}\exp(-k\delta_{BL})\right)},$$

$\varsigma(Y) = \exp(\mathrm{i}5\pi/6)(k_x\tau/\nu)^{1/3}(Y)$ and $\zeta = (1-\mathrm{i})/\sqrt{2}\delta_w$.

A.3. *The diffusive regime*

The solution for ϕ is

$$\phi = C_1\exp(-\mathrm{i}k_yY) + C_2\exp(\mathrm{i}k_yY) + C_3\exp(-kY),\ Y > 0,$$
$$\phi = C_5\exp(-\mathrm{i}k_yY) + C_6\exp(\mathrm{i}k_yY) + C_7\exp(-kY) + C_8\exp(kY),\ -\delta_{BL} < Y < 0.$$

and the coefficients are

$$C_5 = 2\frac{C_3\exp(-\mathrm{i}k_y\delta_{BL})}{\left(\left(-1+\dfrac{\mathrm{i}k_y}{k}\right)+\lambda\left(1+\dfrac{\mathrm{i}k_y}{k}\right)\right)\exp(k\delta_{BL}) + \left(-\left(1+\dfrac{\mathrm{i}k_y}{k}\right)+\lambda\left(1-\dfrac{\mathrm{i}k_y}{k}\right)\right)\exp(-k\delta_{BL})},$$

$$C_6 = -\lambda C_5\exp(\mathrm{i}2k_y\delta_{BL}),$$

$$C_1 = C_5 + \frac{k^2k_x\tau}{\nu k_y\left(k^2+k_y^2\right)^2}(C_5+C_6+C_3),$$

$$C_2 = C_6 - \frac{k^2k_x\tau}{\nu k_y\left(k^2+k_y^2\right)^2}(C_5+C_6+C_3),$$

$$C_7 = -\frac{\exp(-k\delta_{BL})}{2}\left(\left(1+\frac{\mathrm{i}k_y}{k}\right)C_5\exp(\mathrm{i}k_y\delta_{BL}) + \left(1-\frac{\mathrm{i}k_y}{k}\right)C_6\exp(-\mathrm{i}k_y\delta_{BL})\right),$$

$$C_8 = -\frac{\exp(k\delta_{BL})}{2}\left(\left(-1+\frac{\mathrm{i}k_y}{k}\right)C_5\exp(\mathrm{i}k_y\delta_{BL}) - \left(1-\frac{\mathrm{i}k_y}{k}\right)C_6\exp\left(-\mathrm{i}k_y\delta_{BL}\right)\right),$$

where

$$\lambda = \frac{(2k+\alpha)\left(-1+\dfrac{\mathrm{i}k_y}{k}\right)\exp(k\delta_{BL}) + \alpha}{(-2k+\alpha)\left(1+\dfrac{\mathrm{i}k_y}{k}\right)\exp(k\delta_{BL}) + \alpha},$$

$$\alpha = \frac{\mathrm{i}k_x\tau\left(3k^2+k_y^2\right)}{\nu\left(k^2+k_y^2\right)^2}.$$

A.4. *The convective–diffusive regime*

The oscillatory solution near the edge of the boundary layer is

$$\psi_e = C_{e1}\mathrm{e}^{\mathrm{i}k_yY}\left[1+\frac{k_x\tau}{2k_y\nu}\left(\frac{Y^2}{2}-\frac{Y}{2\mathrm{i}k_y}-\frac{1-\mathrm{e}^{-2\mathrm{i}k_yY}}{4k_y^2}\right)\right]$$
$$+ C_{e2}\mathrm{e}^{-\mathrm{i}k_yY}\left[1-\frac{k_x\tau}{2k_y\nu}\left(\frac{Y^2}{2}+\frac{Y}{2\mathrm{i}k_y}-\frac{1-\mathrm{e}^{2\mathrm{i}k_yY}}{4k_y^2}\right)\right], \qquad \text{(A 3)}$$

and the coefficients are

$$C_{e1} = \frac{1}{2}\left(\psi(0) + \frac{1}{\mathrm{i}k_y}\frac{\mathrm{d}\psi}{\mathrm{d}Y}(0)\right),$$

$$C_{e2} = \frac{1}{2}\left(\psi(0) - \frac{1}{\mathrm{i}k_y}\frac{\mathrm{d}\psi}{\mathrm{d}Y}(0)\right),$$

where $\psi(0) = C_5\mathrm{Ai}[\mathscr{Z}(0)] + C_6\mathrm{Bi}[\mathscr{Z}(0)]$ and $(\mathrm{d}\psi/\mathrm{d}Y)(0) = (C_5\mathrm{Ai}'[\mathscr{Z}(0)] + C_6\mathrm{Bi}'[\mathscr{Z}(0)])\mathscr{Z}'$. The constants C_5 and C_6 remain the same as in the exact analytical solution (A 1).

The wall solution is

$$\begin{aligned}\psi_w(Y) = {} & C_{w1}\mathrm{e}^{\mathrm{i}k_w(Y+\delta_{BL})} + C_{w2}\mathrm{e}^{-\mathrm{i}k_w(Y+\delta_{BL})} \\ & + C_{w1}\mathrm{e}^{\mathrm{i}k_w(Y+\delta_{BL})}\left[\frac{k_x\tau}{2k_w\nu}\left(\frac{(Y+\delta_{BL})^2}{2} - \frac{(Y+\delta_{BL})}{2\mathrm{i}k_w} - \frac{1-\mathrm{e}^{-2\mathrm{i}k_w(Y+\delta_{BL})}}{4k_w^2}\right)\right] \\ & + C_{w2}\mathrm{e}^{-\mathrm{i}k_w(Y+\delta_{BL})}\left[-\frac{k_x\tau}{2k_w\nu}\left(\frac{(Y+\delta_{BL})^2}{2} + \frac{(Y+\delta_{BL})}{2\mathrm{i}k_w} - \frac{1-\mathrm{e}^{2\mathrm{i}k_w(Y+\delta_{BL})}}{4k_w^2}\right)\right],\end{aligned}$$

and the coefficients are

$$C_{w1} = \frac{1}{2}\left(\psi(-\delta_{BL}) + \frac{1}{\mathrm{i}k_w}\frac{\mathrm{d}\psi}{\mathrm{d}y}(-\delta_{BL})\right),$$

$$C_{w2} = \frac{1}{2}\left(\psi(-\delta_{BL}) - \frac{1}{\mathrm{i}k_w}\frac{\mathrm{d}\psi}{\mathrm{d}y}(-\delta_{BL})\right),$$

where $\psi(-\delta_{BL}) = C_5\mathrm{Ai}[\mathscr{Z}(-\delta_{BL})] + C_6\mathrm{Bi}[\mathscr{Z}(-\delta_{BL})]$ and $(\mathrm{d}\psi/\mathrm{d}Y)(-\delta_{BL}) = (C_5\mathrm{Ai}'[\mathscr{Z}(-\delta_{BL})] + C_6\mathrm{Bi}'[\mathscr{Z}(-\delta_{BL})])\mathscr{Z}'$.

Appendix B. Coefficient of the two-fluid eigenfunctions

B.1. *The convective–diffusive regime*

The oscillatory solution near the interface is

$$\begin{aligned}\psi_{Be} = {} & C_{e1}\mathrm{e}^{\mathrm{i}k_eY}\left[1 + \frac{k_x\tau_B}{2k_y\nu_B}\left(\frac{Y^2}{2} - \frac{Y}{2\mathrm{i}k_e} - \frac{1-\mathrm{e}^{-2\mathrm{i}k_eY}}{4k_e^2}\right)\right] \\ & + C_{e2}\mathrm{e}^{-\mathrm{i}k_eY}\left[1 - \frac{k_x\tau_B}{2k_e\nu_B}\left(\frac{Y^2}{2} + \frac{Y}{2\mathrm{i}k_e} - \frac{1-\mathrm{e}^{2\mathrm{i}k_eY}}{4k_e^2}\right)\right],\end{aligned} \tag{B 1}$$

and the coefficients are

$$C_{e1} = \frac{1}{2}\left(\psi(0) + \frac{1}{\mathrm{i}k_y}\frac{\mathrm{d}\psi}{\mathrm{d}Y}(0)\right),$$

$$C_{e2} = \frac{1}{2}\left(\psi(0) - \frac{1}{\mathrm{i}k_y}\frac{\mathrm{d}\psi}{\mathrm{d}Y}(0)\right),$$

where $\psi(0) = C_9\mathrm{Ai}[\mathscr{X}(0)] + C_{10}\mathrm{Bi}[\mathscr{X}(0)]$ and $(\mathrm{d}\psi/\mathrm{d}Y)(0) = (C_9\mathrm{Ai}'[\mathscr{X}(0)] + C_{10}\mathrm{Bi}'[\mathscr{X}(0)])\mathscr{X}'$. The constants C_9 and C_{10} remain the same as in the exact analytical solution (4.9). Here $k_e = \sqrt{(\nu_T/\nu_B)(k_x^2+k_y^2+k_z^2) - (k_x^2+k_z^2)}$.

The wall solution is

$$\begin{aligned}\psi_{Bw} = {} & C_{w1}\mathrm{e}^{\mathrm{i}k_w(Y+\delta_{BL})} + C_{w2}\mathrm{e}^{-\mathrm{i}k_w(Y+\delta_{BL})} \\ & + C_{w1}\mathrm{e}^{\mathrm{i}k_w(Y+\delta_{BL})}\left[\frac{k_x\tau_B}{2k_w\nu_B}\left(\frac{(Y+\delta_{BL})^2}{2} - \frac{(Y+\delta_{BL})}{2\mathrm{i}k_w} - \frac{1-\mathrm{e}^{-2\mathrm{i}k_w(Y+\delta_{BL})}}{4k_w^2}\right)\right] \\ & + C_{w2}\mathrm{e}^{-\mathrm{i}k_w(Y+\delta_{BL})}\left[-\frac{k_x\tau_B}{2k_w\nu_B}\left(\frac{(Y+\delta_{BL})^2}{2} + \frac{(Y+\delta_{BL})}{2\mathrm{i}k_w} - \frac{1-\mathrm{e}^{2\mathrm{i}k_w(Y+\delta_{BL})}}{4k_w^2}\right)\right],\end{aligned}$$

and the coefficients are

$$C_{w1} = \frac{1}{2}\left(\psi(-\delta_{BL}) + \frac{1}{\mathrm{i}k_w}\frac{\mathrm{d}\psi}{\mathrm{d}y}(-\delta_{BL})\right),$$
$$C_{w2} = \frac{1}{2}\left(\psi(-\delta_{BL}) - \frac{1}{\mathrm{i}k_w}\frac{\mathrm{d}\psi}{\mathrm{d}y}(-\delta_{BL})\right),$$

where $\psi(-\delta_{BL}) = C_9\mathrm{Ai}[\mathscr{X}(-\delta_{BL})] + C_{10}\mathrm{Bi}[\mathscr{X}(-\delta_{BL})]$ and $(\mathrm{d}\psi/\mathrm{d}Y)(-\delta_{BL}) = (C_9\mathrm{Ai}'[\mathscr{X}(-\delta_{BL})] + C_{10}\mathrm{Bi}'[\mathscr{X}(-\delta_{BL})])\mathscr{X}'$. Here

$$k_w = \sqrt{(\nu_T/\nu_B)\left(k_x^2 + k_y^2 + k_z^2\right) - \left(k_x^2 + k_z^2\right) + \mathrm{i}(k_x\tau_B\delta_{BL}/\nu_B L)}.$$

REFERENCES

Belcher, S. E. & Hunt, J. C. R. 1998 Turbulent flow over hills and waves. *Annual Rev. Fluid Mech.* **30**, 507–538.

Berger, S. A. & Aroesty, J. 1977 'e^9': stability theory and boundary layer transition. *Tech Rep.* R-1898-ARPA Rand Corporation.

Butler, K. M. & Farrell, B. F. 1992 Three dimensional optimal perturbation in viscous shear flow. *Phys. Fluids* A **4**, 1637–1650.

Charru, F. & Hinch, E. J. 2000 'Phase diagram' of interfacial instabilities in a two-layer Couette flow and mechanism of the long-wave instability. *J. Fluid Mech.* **414**, 195–223.

Craik, A. 1991 The continuous spectrum of the Orr–Sommerfeld equation: note on a paper of Grosch and Salwen. *J. Fluid Mech.* **226**, 565–571.

Grosch, C. E. & Salwen, H. 1978 The continuous spectrum of the Orr–Sommerfeld equation. Part 1. The spectrum and the eigenfunctions. *J. Fluid Mech.* **87**, 33–54.

Hernon, D., Walsh, E. J. & McEligot, D. M. 2007 Experimental investigation into the routes to bypass transition and the shear-sheltering phenomenon. *J. Fluid Mech.* **591**, 461–479.

Hooper, A. P. & Boyd, W. G. C. 1983 Shear-flow instability at the interface between viscous fluids. *J. Fluid Mech.* **128**, 507–528.

Hooper, A. P. & Boyd, W. G. C. 1987 Shear-flow instability due to a wall and a viscosity discontinuity at the interface. *J. Fluid Mech.* **179**, 201–225.

Hunt, J. C. R. 1977 A review of rapidly distorted turbulent flows and its applications. *Fluid Dyn. Res.* **9** (01), 121–152.

Hunt, J. C. R. & Durbin, P. A. 1999 Perturbed vortical layers and shear sheltering. *Fluid Dyn. Res.* **24** (06), 375–404.

Jacobs, R. G. & Durbin, P. A. 1998 Shear sheltering and the continuous spectrum of the Orr–Sommerfeld equation. *Phys. fluids* **10** (8), 2006–2011.

Jacobs, R. G. & Durbin, P. A. 2001 Simulations of bypass transition. *J. Fluid Mech.* **428**, 185–212.

Jordinson, R. 1971 Spectrum of eigenvalues of the Orr–Sommerfeld equation for Blasius flow. *Phys. fluids* **14** (11), 2535–2537.

Mack, L. M. 1976 A numerical study of the temporal eigenvalue spectrum of the Blasius boundary layer. *J. Fluid Mech.* **73**, 497–520.

Maslowe, S. A. & Spiteri, R. J. 2001 The continuous spectrum for a boundary layer in a streamwise pressure gradient. *Phys. fluids* **13**, 1294–1299.

Morkovin, M. V. 1969 *Viscous Drag Reduction*. Plenum.

Nakamura, L., Kershaw, R. & Grait, N. 1996 Prediction of near-surface gusts generated by deep convection. *Meteorol. Appl.* **3**, 157–167.

Nelson, J. J., Alving, A. E. & Joseph, D. D. 1995 Boundary layer flow of air over water on a flat plate. *J. Fluid Mech.* **284**, 159–169.

Orszag, S. A. 1971 Accurate solution of the Orr–Sommerfeld stability equation. *J. Fluid Mech.* **50** (4), 689–703.

Salwen, H. & Grosch, C. E. 1981 The continuous spectrum of the Orr–Sommerfeld equation. Part 2. Eigenfunction expansions. *J. Fluid Mech.* **104**, 445–465.

Schlichting, H. 1933 Berechnung der Anfachung kleiner Störungen bei der Plattenströmung. *ZAMM* **13**, 171–174.

Schlichting, H. 1987 *Boundary-Layer Theory*, 7th ed. McGraw-Hill.

Tollmien, W. 1929 Über die Entstehung der Turbulenz. *Nachr. Ges. Wiss. Göttingen* **1**, 21–44.

Tumin, A. 2003 Multimode decomposition of spatially growing perturbations in a two-dimensional boundary layer. *Phys. Fluids* **15** (9), 2525–2540.

Yecko, P. & Zaleski, S. 2005 Transient growth in two-phase mixing layers. *J. Fluid Mech.* **528**, 43–52.

Yih, C. S. 1967 Instability due to viscosity stratification. *J. Fluid Mech.* **27**, 337–352.

Zaki, T. A. & Durbin, P. A. 2005 Mode interaction and the bypass route to transition. *J. Fluid Mech.* **531**, 85–111.

Zaki, T. A. & Durbin, P. A. 2006 Continuous mode transition and the effects of pressure gradient. *J. Fluid Mech.* **563**, 357–388.